COLLISION BROADENING USING ALKALI-FILLED, HOLLOW CORE FIBERS

THESIS

Luke P. Rodgers, Second Lieutenant, USAF

AFIT/GAP/ENP/07-S01

DEPARTMENT OF THE AIR FORCE
AIR UNIVERSITY

AIR FORCE INSTITUTE OF TECHNOLOGY

Wright-Patterson Air Force Base, Ohio

The views expressed in this thesis are those of the author and do not reflect the official policy or position of the United States Air Force, Department of Defense, or the United States Government.

AFIT/GAP/ENP/07-S01

COLLISION BROADENING USING ALKALI-FILLED, HOLLOW CORE FIBERS

THESIS

Presented to the Faculty

Department of Engineering Physics

Graduate School of Engineering and Management

Air Force Institute of Technology

Air University

Air Education and Training Command

In Partial Fulfillment of the Requirements for the

Degree of Master of Science (Applied Physics)

Luke P. Rodgers, B.S.

Second Lieutenant, USAF

September 2007

AFIT/GAP/ENP/07-S01

COLLISION BROADENING USING ALKALI-FILLED, HOLLOW CORE FIBERS

Luke P. Rodgers, B.S.

Second Lieutenant, USAF

Approved:

Timothy H. Russell (Chairman)	15 OCT 2007 Date
Glenn P. Perram (Member)	15 OCT 2007 Date
David E. Weeks (Member)	15 Oct 2007 Date

Abstract

The goal of this research was to demonstrate the possibility of collision broadening in a cesium-filled, hollow-core fiber as an alternative to the proven technique of pressure broadening. Theoretically, alkali electrons should relax from the $^2P_{3/2}$ to the $^2P_{1/2}$ level and the absorption spectrum should collisionally broaden due to the presence of fiber walls, as opposed to the more common pressure broadening method. An absorption dip located at 852.34nm was recorded in a pressure broadened comparison leg. This data was used as a baseline during analysis of the fiber leg's data.

While the fiber was successfully exposed to the cesium under safe, controlled conditions, unexpected fluctuation in both the coupling efficiency and laser power levels resulted in the inability to record an absorption dip in the final data. As a result, an investigation of the fundamental assumptions and theory supporting this experiment was conducted. It was discovered that the current design does not provide an adequate opportunity for cesium to make its way into the fiber core, thus negating the possibility of achieving the desired collision broadening data. Recommendations are made as to how to improve this experiment for future study, founded on both theoretical calculations and experience gained in the lab.

This research does not provide evidence of the ability to fill hollow-core fibers with alkali gas. Rather, it exposes the complexity of putting the theory of collisional broadening into practice and provides suggestions on how to succeed in the next attempt.

Acknowledgements

I would like thank Maj Tim Russell for his guidance and extraordinary patience throughout this entire project. Maj Steve Massey deserves endless thanks from both myself and the larger research community for lending me his lab expertise on a daily basis, without which disaster would have surely resulted. Other lab catastrophes were avoided with the brilliant assistance of Greg Pitz, Mike Ranft, and Greg Smith. Our talented glassblower, Mike Ray, was able to create exactly what we wanted despite our vague descriptions. Theoretical roadblocks were deftly cleared by the incomparable Dr Glen Perram and Dr David Weeks. John Callahan, Capt Ryan Givens, Mark Spencer, and Capt Justin Spring all helped me to look at problems in different ways, which didn't always help but nevertheless provided some variety. Lastly, I should thank my family and friends for keeping me on track.

Table of Contents

List of Figures

COLLISION BROADENING USING ALKALI-FILLED, HOLLOW CORE FIBERS

I. Introduction

The multitude of applications using some form of a laser is staggering, but one of the most significant has not yet been realized. A high-energy laser (HEL) which can be directed and aimed is the ultimate weapon of the 21st century, and with each technological advance it becomes more achievable goal than science fiction cliché.

The motivation is obvious. A HEL can provide the war fighter with a weapon of unmatched precision, potentially eliminating collateral damage from the military's lexicon. Yet there are currently two competing schools of thought debating the best way to achieve this goal. One is to base the weapon on a diode-pumped solid-state laser (DPSSL) while the other is a chemically-pumped gas laser. Both options have their own pros, the most obvious being the pumping mechanism of the solid-state lasers and the medium of the gas lasers, but they are not without their cons. Although the chemically-pumped gas laser has demonstrated greater power levels, it uses very reactive and potentially dangerous chemicals that are not easily re-supplied. The diode pump of the solid-state laser, on the other hand, is electrically powered, providing plenty of viable options for battlefield packaging. Unfortunately, the solid-state laser cannot currently generate the desired levels of power and beam quality. The crystals used in solid-state lasers all have a thermal limit at which damage will be incurred or the beam quality will be severely degraded. The gaseous medium may be able to solve the thermal management problem, as it is foreseeable that cycling out the gas as it heats up could ameliorate thermal degradation. In other words, the diode pump of the solid-state lasers is

most applicable to the battlefield while the gaseous medium of the chemical lasers gives us the best power and beam quality.

Therefore, it makes sense to combine the two best pieces of differing HEL research approaches into one hybrid system, theoretically achieving superb photon engine efficiency (quantum efficiency $\eta = 95 - 99\%$ with generation of $10^8 \frac{\text{photons}}{\text{atom} \cdot \text{second}}$). [12] Still, the issue of spectrally matching the absorption in the gas medium with the pump source remains. Primarily, diode pumps generally produce a spectrally diverse output and much of that power is wasted due to a thin Gaussian absorption profile on the part of the gas. One thought is to use pressure broadening to widen the absorption bandwidth of the gas. This is a legitimate approach, but a substantial amount of pressure is required for the desired level of broadening, which in turn creates more problems to be solved. If we could limit the necessary broadening by narrowing the bandwidth of the pump source, however, some of these problems could be alleviated. Realistically, the main challenge to overcome is the broadening already mentioned.

This thesis investigates the plausibility of combining a photonic crystal fiber (PCF) and a diode pumped alkali laser (DPAL). A hollow core fiber filled with the alkali gas (in this case cesium) will act as the optical cavity. The main goal of this experiment is to determine whether Cs can be introduced into a hollow core fiber. One piece of evidence that would support the plausibility of this goal is a noticeable absorption spectrum for Cs after a range of frequencies is propagated through the gas-filled fiber. The intention is to achieve line broadening by way of collisions between gaseous Cs and the fiber wall as opposed to pressure. Typically, a significant amount of pressure is required in order to match the absorption bandwidth with the diode pump. The PCF,

while acting as a cavity of sorts, should cause broadening due to the elastic collisions of Cs with the walls. The collisional broadening due to the presence of the PCF walls will provide another option for broadening; most importantly one that does not require any additional added pressure. Also, where a typical solid-core fiber can currently only handle about 500W, due to non-linear effects, the introduction of an alkali gas into the core suggests the possibility of kilowatt levels within one fiber element. Continued research will surely improve this output for the solid-core fibers, but those same research efforts could instead be focused on increasing the efficiency of kilowatt hollow-core fibers. This is a very promising idea when looking ahead to the actual application in a HEL.

Chapter II of this thesis will supply the reader with the pertinent information necessary to understand the research challenges and goals. Chapter III will outline the experimental setup along with detailed description of the equipment used at each step. Chapter IV will present all the findings yielded from this research, along with an in-depth analysis of both recorded data and suggestions for alterations if follow-on projects are undertaken. Finally, Chapter V will sum up the progress made during this experiment as well as provide thoughts on continuation.

II. Theoretical Background

Chapter II presents some of the basic concepts necessary to understand the overall research goals, specifically an introduction to laser spectroscopy and a review of fiber optic theory.

2.1 Laser Spectroscopy

Though heavily rooted in science fiction, the term laser is actually a fairly descriptive acronym: Light Amplification by Stimulated Emission of Radiation. Each word contributes a meaningful piece to the explanation of this technology. Understanding lasers and spectroscopy is akin to a "chicken or the egg" argument, as one topic is heavily linked to the other, but in this case it is best to start with atomic spectroscopy.

Dealing with energy levels and electron excitation can be a complex task, but it can be simplified enough for this particular context without losing any critical points. Some quantum mechanics are required, most importantly the equation

$$E = h\nu \tag{2.1}$$

which shows that energy of a photon, E, is based on Plank's constant, h, and the frequency of the light, ν. For simplicity's sake, we'll consider a hydrogen atom with one electron in its ground, or natural, unexcited state. If an electromagnetic wave comes into contact with our hydrogen atom and one of its photons possesses the exact amount of energy, based on Equation 2.1, needed to excite the electron to the next energy level then the hydrogen atom will absorb that photon's energy and the electron will move up. The electron will not remain there indefinitely, and eventually will return to its ground state. As the electron returns to the ground state, the extra energy will be reradiated in the form

of a new photon, once again based on Equation 2.1. Figure 2.1 illustrates an extremely elementary version of this concept.

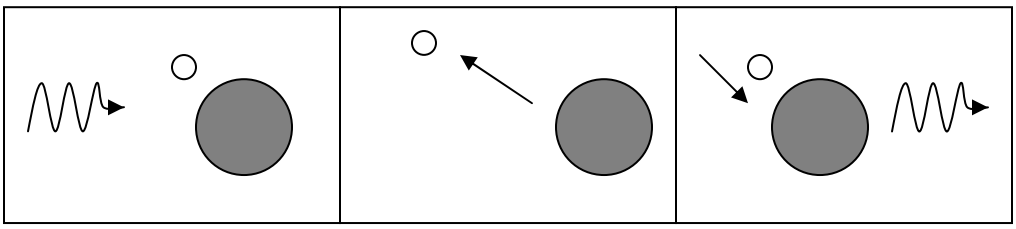

Figure 2.1. Photon absorption and re-emission. Light is absorbed by an atom. Electrons are excited to a higher energy level. Finally, the electrons return to the ground state, simultaneously emitting a new electromagnetic wave.

Spectroscopy is the study of atoms or molecules absorbing and reemitting light waves, where both processes are unique to the atom or molecule under investigation. Another way to visualize this is with an energy level diagram, like the basic one in Figure 2.2.

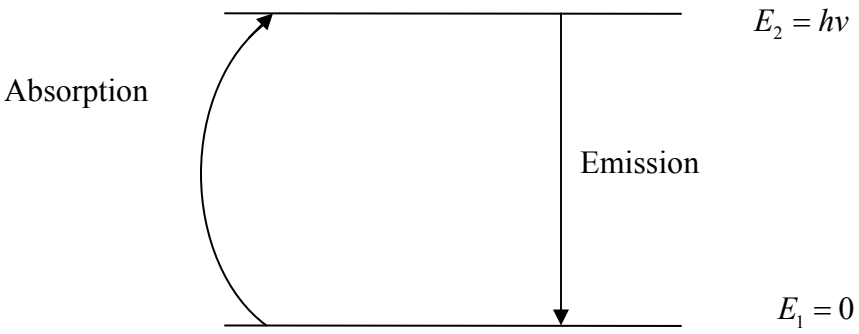

Figure 2.2. Simplified visualization of absorption and emission.

The process of emission is much more complicated than the diagram suggests, as there are both stimulated and spontaneous emissions. The spontaneous emission is dictated by

$$\frac{\partial N_{2spont}}{\partial t} = -A_{21} N_2 \tag{2.2}$$

where N_{2spont} is the number of atoms in the second energy state and A_{21} is the proportionality constant, also known as the Einstein A coefficient. The proportionality

constant relates the two energy levels in question, this case being one and two. Stimulated emission is defined similarly as

$$\frac{\partial N_{2stim}}{\partial t} = -B_{21}\rho(v)N_2 \tag{2.3}$$

where the new variables are B_{21}, the Einstein B coefficient, and $\rho(v)$, the radiation density of photons at frequency *v*. The radiation density factors in how many photons are being used to "stimulate" emission, whereas spontaneous emission does not depend on any external factors.

It is now possible to describe the physical design of a generic laser. Any laser has a pump source and a gain medium contained in an optical cavity, as shown in Figure 2.3.

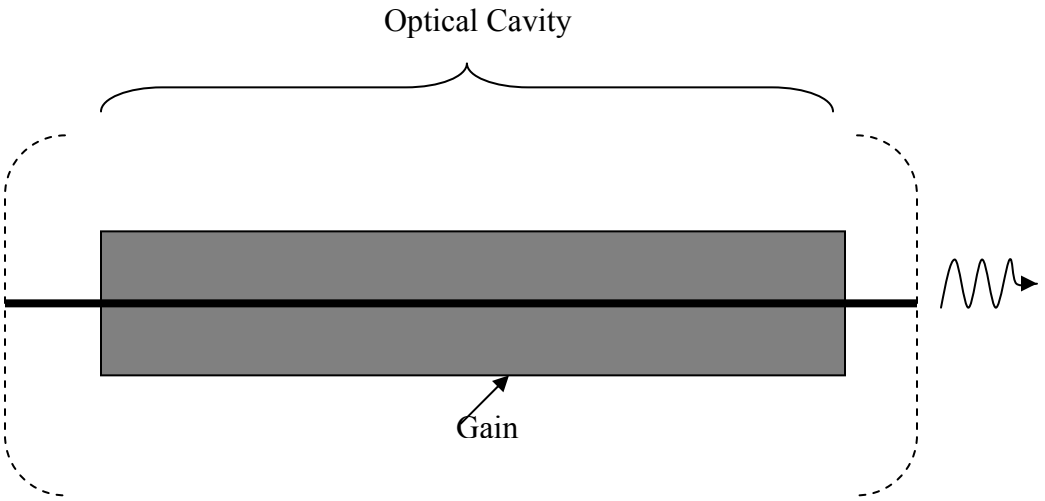

Figure 2.3. Every laser design will include an optical cavity and a gain medium. Specific types will yield different power levels and wavelengths.

The gain medium, also called the active laser medium, can be a crystal, a gas, or even a liquid. The gain medium is excited by an external pump source, which transfers energy to the gain medium in the form of electricity, light, or a chemical reaction. This portion is best represented by Figure 2.2 as absorption. At a specific energy level the photons will

be absorbed by the atoms in the gain medium; thus pushing the gain medium's outer shell electrons into higher energy levels. Eventually, there will be more particles in high-energy states than the original states. This arrangement is referred to as a population inversion, characterized by more emission than absorption. In other words, the pump is still exciting the low energy particles but now we have a constant supply of excited atoms which can emit energy in the form of single wavelength light. All of this light is in-phase and has the same polarization, something that will be explained in more depth in the optics section.

This coherent beam is repeatedly reflected off the ends of the optical cavity, amplifying the signal with each pass, before it finally exits the cavity in the form of a laser beam. Ideally, a laser beam is near-monochromatic; meaning that only one wavelength of light is generated. One can compare this to an everyday light bulb, which produces light over a wide range of wavelengths. Also, whereas a laser directs the coherent beam in one particular direction a light bulb allows the photons out in almost every direction. Granted, if the laser beam exits into free space it will appear as a Gaussian and will exhibit some divergence, but this can be remedied by propagating through a waveguide, such as an optical fiber.

These new details shed more light on the previously given equations and figures, hopefully illuminating some of the finer points. Population inversion fundamentally means there are more atoms in an excited state than in a lower energy level, which then translates to a steady transition from the excited state to the lower energy level, described in Equation 2.3. Also, a modification of Figure 2.2 is to be expected, seen in Figure 2.4 as a three-level system, since straight two-level systems are not possible. [17]

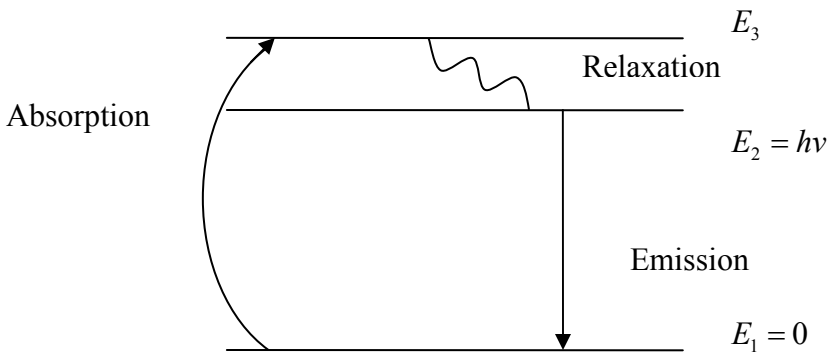

Figure 2.4. The more common type of laser utilizes the gain medium's absorption of the pump energy and a relaxation to the desired excited level, which yields emission at a desired wavelength.

Often, the gain medium absorbs the pump energy, but the excited atoms then relax to a different, slightly lower excited state. This process is appropriately named relaxation, and emission follows via the $E_2 \rightarrow E_1$ transition. The point to take away from this clarification is that the emitted wavelength will be different, based on the quantum relation of energy to frequency in Equation 2.1. For our particular research, we were most concerned with the cesium energy level diagram, which can be seen in Figure 2.5.

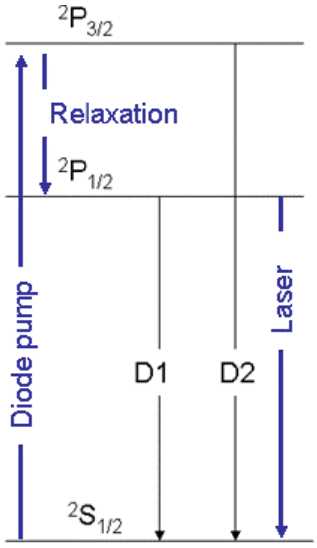

Figure 2.5. Cesium energy level diagram. The D1 and D2 lines describe the hyperfine structure. [12]

An ancillary topic that was touched upon in the introduction concerns spectrally matching the gas medium to the pump source. This is best explained in conjunction with Figure 2.6, which illustrates the ambiguous description of broadening the absorption bandwidth. By widening the gas medium absorption with increased pressure it will match up with the pump source's power, maximizing the absorption of the pump. Another option for this is the aforementioned collision broadening, in which the walls of the cavity cause elastic collisions that result in broadening.

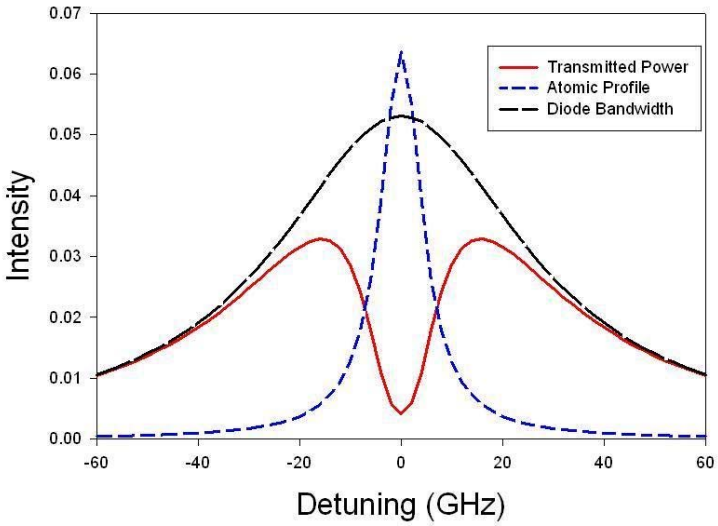

Figure 2.6. Gas phase distribution compared to the diode distribution. If the atomic profile can be broadened or the diode bandwidth can be narrowed to more closely match each other, power will increase. [12]

Knowledge of lasers and spectroscopy allows for a plethora of interesting applications. By stimulating an atom and observing what wavelengths of light are emitted, it is possible to classify and categorize elements in the periodic table based only on absorption and emission spectra.

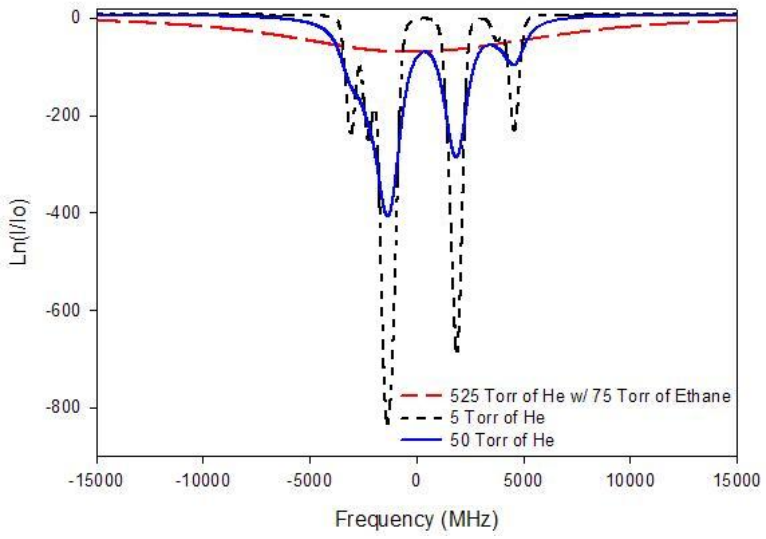

Figure 2.7. Spectral data displays dips at the frequency that light is absorbed. This example also illustrates broadening. [12]

If one wanted to detect the presence of a particular element in a container, it would only require recording power levels while sending laser light at an appropriate wavelength through that container. If a power dip occurs when scanning through a range of wavelengths, and that dip corresponds to the wavelength absorbed by the element in question, then the element is present.

2.2 Fiber Optics

When considering the broad field of optics, few subcategories have garnered more attention in recent years than that of fibers. The idea of guiding light along essentially any conceivable path is clearly an attractive pursuit, hinting at a multitude of applications.

Total Internal Reflection (TIR) is the fundamental principle of operation for traditional optical fibers. Basic optics tells us that light will bend as it propagates from a medium of one index of refraction into a medium with a different index of refraction, as seen in Figure 2.8.

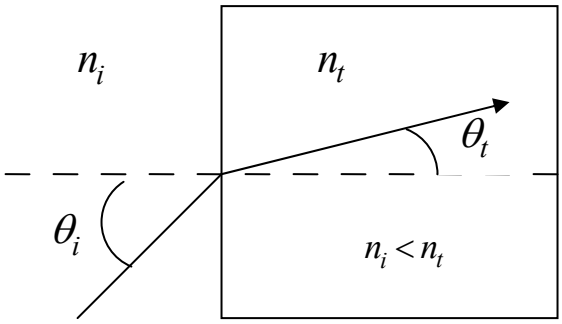

Figure 2.8. Snell's Law defines how light refracts at interfaces.

This concept is known as Snell's Law

$$n_i \sin\theta_i = n_t \sin\theta_t \tag{2.4}$$

where n_i and θ_i are the incident medium's index of refraction and angle, respectively, with logical subscript modifications made for the transmitted medium versions (n_t and θ_t). If we take the case of light making its way from a higher index, typically referred to as the core, into a lower index, known as the cladding, all of the incident light will reflect back into the higher index region if the incident angle is within a certain range. The lower limit of this range is known as the critical angle, and may be found by

$$\theta_c = sin^{-1}\frac{n_t}{n_i} \tag{2.5}$$

where n_t the index of refraction for the lower index material, n_i is the index of the incident medium, and θ_c is the critical angle as measured from the normal of the index boundary. Upon meeting these criteria, the light will continually reflect inside the core, making its way down the fiber unaltered with respect to wavelength and with potentially minimal loss determined by the material makeup of that particular fiber. Figure 2.9 illustrates the concept of TIR.

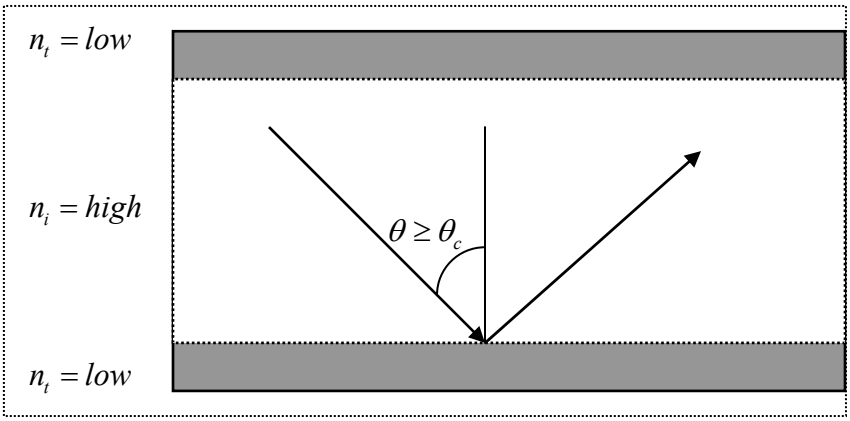

Figure 2.9. Total internal reflection with two boundaries.

Keep in mind that this example is easily expanded into three dimensions. If one were to take the two-dimensional slab and rotate it along the central z-axis a three-dimensional cylinder would result, retaining the same indicial properties and now allowing for circular propagation as opposed to a strictly linear containment; thus, we have an optical fiber, as represented in Figure 2.10.

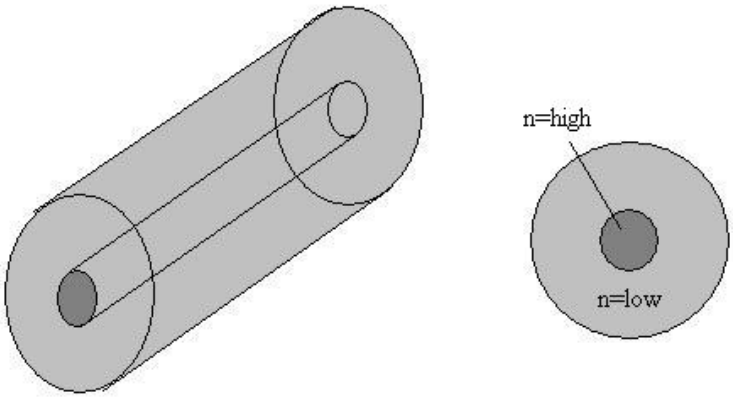

Figure 2.10. Generic optical fiber perspectives.

Now that the basic foundation for understanding the field of optical fibers has been laid, it is necessary to expand on some more specficic accompanying theory. Of the distinguishing characteristics of optical fibers, one of the most substantial is the classification as a multi-mode or single-mode fiber. A mode is one particular way light

can propagate through a fiber, where a high-order mode propagates with a larger angle and a low-order mode maintains a more shallow propagation path. The path length can be found by

$$l = L / cos\theta_t \tag{2.6}$$

where L is the fiber length and θ_t is the angle from the z-axis. Figure 2.11 demonstrates how this difference in path length, along with a π radian phase shift upon each internal reflection of a high-to-low index interface, can cause differences in when the various modes cross the same point in the fiber. Keep in mind that this is only using the ray-description of light, while the wave properties are a completely different issue. This becomes most important when considering that the various modes exit the fiber at different times despite entering simultaenously. This "de-synching" of the modes is called intermodal dispersion.

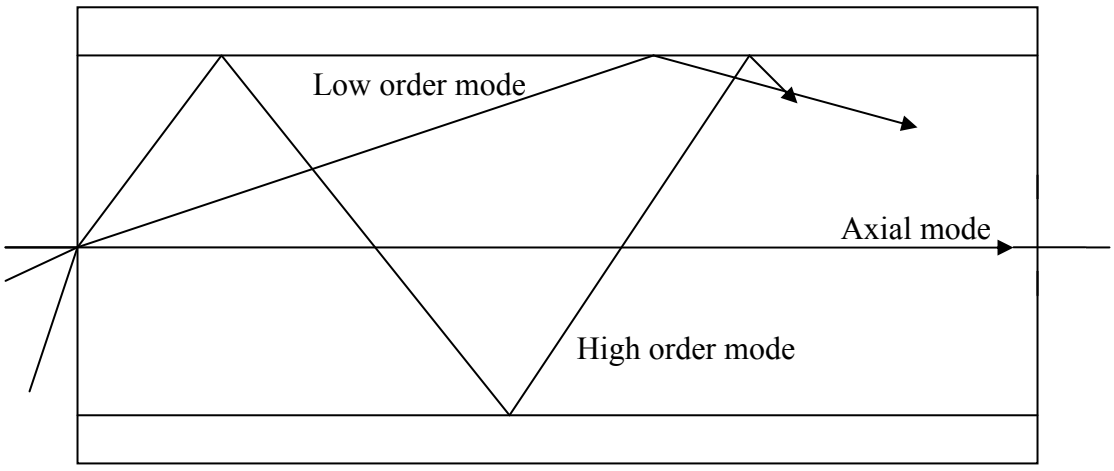

Figure 2.11. Intermodal dispersion in a multi-mode optical fiber.

Over short distances intermodal dispersion does not require much consideration, but when long-distance communications are involved it can make a significant difference. For example, if bundles of information are sent through a multimode optical fiber, the

receiver will see higher order modes from some bundles at the same time as lower order modes from other bundles sent at different times. In other words, the original transmission becomes garbled.

An alternative to the multi-mode fibers is the appropriately named single-mode fiber. The difference between the multimode and single-mode fibers can be explained by the size of the core diameter and the numerical aperture (NA), which will be addressed later. Multi-mode cores are typically larger than 10μm while single-mode cores are smaller than 10μm. Essentially, whereas a large core can allow multiple modes at various incident angles, a small core makes it imperative to precisely align the light source to achieve near-axial light propagation. Unintended modes will either never make it into the core or will leak into the cladding and out of the fiber, both of which are a result of the smaller core and the original TIR criteria.

The TIR-based fibers discussed thus far are not the only option in the field and are seeing increased competition from another type of fiber which yields similar results but with an entirely different theoretical basis. A photonic-crystal fiber (PCF) is a fiber which utilizes the concepts of a photonic-bandgap (PBG) and Bragg's Law, the latter of which can be represented as

$$2d\sin\theta = m\lambda \tag{2.7}$$

where d is one material's layer width, θ is the angle of incidence, λ is the wavelength of the light, and m is an integer. Bragg's Law is most easily understood when related to a Bragg grating, which is made up of layered alternating indices of refraction where each layer's thickness is determined by the d in Bragg's law. The basic idea behind a Bragg grating is that any incident beam will be partially transmitted and partially reflected at an

interface, save for the TIR case which we are not concerned with in this situation. By appropriately choosing the thickness of the layers, one can achieve a special result: all the reflected beams will be in-phase regardless of how many layers were crossed. Figure 2.12 demonstrates this concept.

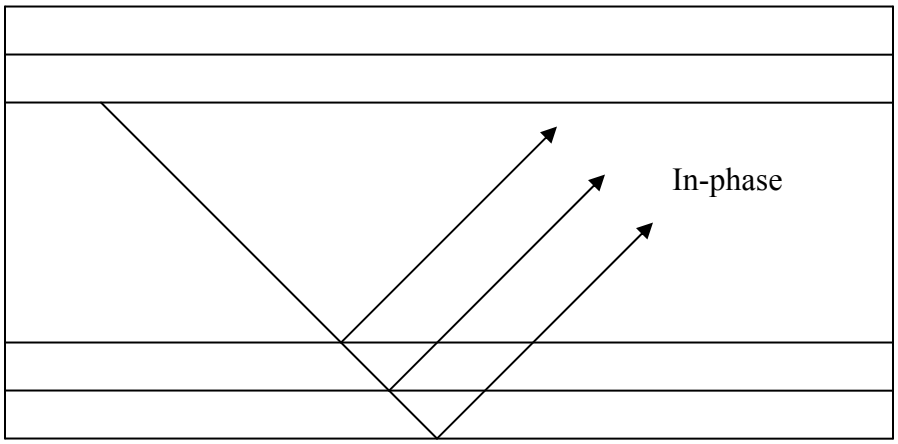

Figure 2.12. A photonic crystal fiber based on a Bragg grating.

The key to the Bragg grating, and therefore to some PCFs, is the integer multiple of the wavelength concerned. The path lengths for each reflected beam after the initial interface have some additional uniform distance. For certain thicknesses and incident angles, this presents multiple signals that took different routes but arrive at the same point in phase.

Some PCFs use photonic bandgaps as the limiting nature of these gratings, such that only certain wavelengths are able to propagate through the fiber. A defect in the photonic crystal guides certain wavelengths corresponding to a bandgap, while the periodic material surrounding the defect filters out other wavelengths.

Based on the given description, it seems natural to imagine a PCF as a series of concentric cylinders, but another popular design is one that bundles those cylinders into a larger cylinder, as seen in Figure 2.13.

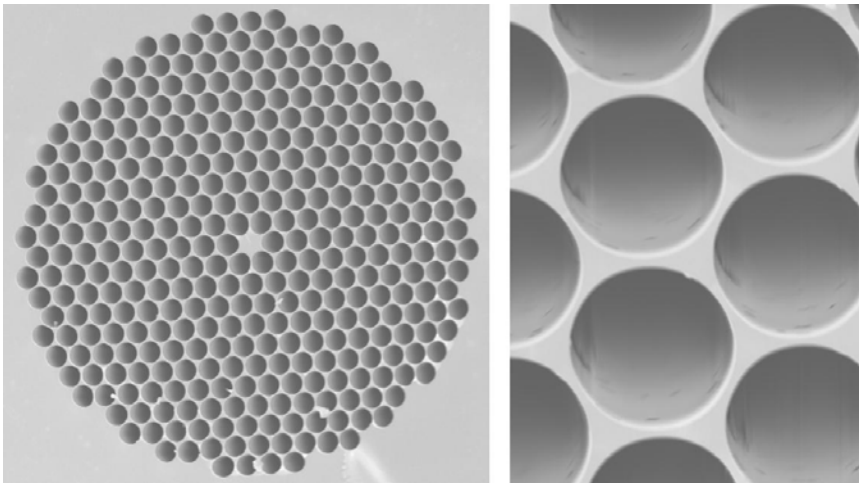

Figure 2.13. “SEM micrographs of a photonic-crystal fiber produced at US Naval Research Laboratory. (left) The diameter of the solid core at the center of the fiber is 5μm, while (right) the diameter of the holes is 4μm.” [1]

A solid-core fiber can still work based on TIR, since the core is of a higher index than the surrounding holes, but the more substantial contrast between the core and air allows for better results in applications involving non-linear effects and where polarization is a concern. Specifically, the normal component of the electric field takes on a π radian phase shift upon each internal reflection of a high-to-low index interface.

The PCF approach, based on bandgaps, does not need to meet the same indicial and angular requirements as TIR, therefore allowing for a variety of otherwise impossible fiber designs. A PCF can have a core index which is lower than the surrounding cladding. Any light that is transmitted will meet interface after interface, continually reflecting portions of the signal in-phase with the initial interface’s reflection. Given that the layer thickness is most crucial in achieving constructive interference, specific indicial ratios are chosen to yield desired results and performance given the wavelength and fiber length. An option using one extreme of the index spectrum is to make a hollow-core fiber (HCF), or holey-fiber. This entails a large hollow core and surrounding smaller hollow cylinders.

A HCF is identical to Figure 2.12 with no material in the center. The possibilities offered by HCFs are constantly expanding, the most obvious being the option to put something inside the fiber, such as a gas. As most of the mode is present in air as opposed to some other material, HCFs provide numerous advantages over solid-core fibers, including reduced absorption loss and non-linear effects. These qualities are very attractive in those applications where high power levels are desired.

Regardless of the type of fiber involved, the initial and most taxing challenge is actually getting light into the fiber correctly, more commonly refered to as coupling. The simplest explanation of this process is based on typical TIR fibers, where we need only consider a cladding index and a core index. Starting with Equation 2.5, we can substitute the subscripts to specify cladding, n_c, and fiber core, n_f, and rearrange everything with trigonometric techniques. Figure 2.14 illustrates the pertinent angles.

$$sin\theta_c = \frac{n_c}{n_f} = sin(90^\circ - \theta_t) \tag{2.8}$$

$$\frac{n_c}{n_f} = cos\theta_t = \sqrt{1 - sin^2\theta_t} \tag{2.9}$$

At this point, we can square both sides and use Snell's Law to find the maximum incident angle that satisfies the transmitted angle's restrictions.

$$1 - \frac{n_c^2}{n_f^2} = sin^2\theta_t \tag{2.10}$$

$$n_f^2 - n_c^2 = n_f^2 sin^2\theta_t = n_i^2 sin^2\theta_i \tag{2.11}$$

$$sin\theta_i = \frac{1}{n_i}\sqrt{n_f^2 - n_c^2} \tag{2.12}$$

The θ_i can be considered to be $\theta_{\max}$ for the indices in question. If we employ the small angle approximation, which states that for near-axis rays we can assume:

$$sin\theta \cong \theta \tag{2.13}$$

then the sine expressions are eliminated. This simplification is logically sound given that we are working at near-axis angles. Finally, we assume the incident medium is air and thus we have the NA, a common variable used in the fiber industry, as seen in Equation 2.14.

$$NA = \sqrt{n_f^2 - n_c^2} \tag{2.14}$$

Along with core size, the square of the numerical aperture is an easy way to compare multiple systems' ability to gather light and is often provided with other fiber specifications by the manufacturer. Once again, it is not required to use the exact angle to achieve a specified NA, but rather to couple in at a shallower angle than the NA.

This does not seem like a daunting task initially, but once the light source is factored in to the situation it gets slightly more complicated. Ideally, a ray of light with negligible width would simply need to approach the fiber at an angle that is smaller than $\theta_{\max}$, which is related to θ_c. However, this is not the actual case, as even laser light beams have a measurable width. As mentioned earlier, fiber cores are roughly 10μm in diameter whereas many lasers produce beams on the order of millimeters. Thus, it is necessary to focus the laser beam down to a point at a specific angle as determined by the NA.

$$tan(NA) = \frac{D}{2f} \tag{2.15}$$

mathematically describes the relation between NA, the beam width before focusing, *D*, and the microscope focal length, *f*, while Figure 2.14 provides a visual representation of this concept.

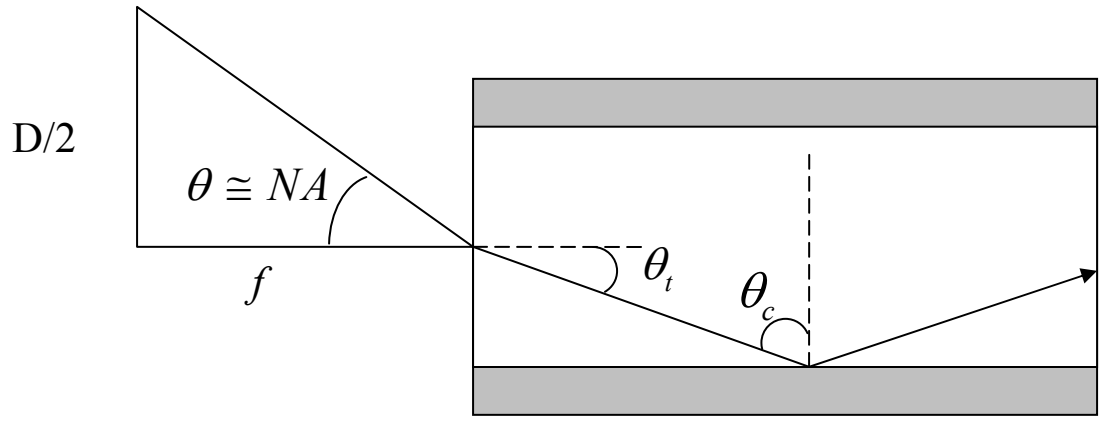

Figure 2.14. Beam width must be modified, often with a microscope objective, in order to successfully couple light into a fiber.

This allows for some options in experiment design as one can alter the beam width or the microscope objective to achieve coupling for a certain fiber.

2.3 Useful Optical Devices

Coupling light into a fiber is challenging enough in itself, but there are some common optical devices that can make this step less headache-saturated. This section will combine any relevant theory with the more straightforward engineering issues.

To follow up on the discussion of beam width and NA, a laser source may not even be usable with standard microscope objectives if it is too broad. In these cases, it is necessary to use a telescope to alter the source beam, which is just another way to say magnification based on lenses. The equations

$$d = f_1 + f_2 \tag{2.16}$$

$$M = \frac{f_1}{f_2} \tag{2.17}$$

are all that is needed to design a telescope for most situations, where d is the distance between the two lenses, the f's are each lens' focal length, and M is the achieved magnification. For example, if one needed a 2x magnification, all they would need to do is satisfy the ratio to get $M = 2$. Granted, it is not really that simple, seeing as the order and type of lens is critical. To enlarge a collimated beam, one could use a concave planar lens to diverge the source beam and then a biconvex lens to re-collimate the beam. Thus, a little finesse and sometimes luck is necessary to find available lenses that both meet the magnification requirements and minimize the amount of effort needed to optimize the distance between the lenses.

The magnification just discussed assumes spherical lenses, either concave or convex, but another telescope worth mentioning is one that employs cylindrical lenses. Cylindrical lenses are only curved along one axis, and thus they do not create uniform magnification along all axes. This is very useful for elliptical beams. For example, if a laser beam source is measured to be twice as long along the y-axis as it is along the x-axis, it is easily changed into a circular beam with the help of a cylindrical telescope where either the magnification of the y-axis is 0.5 or the magnification of the x-axis is two.

The last relevant optics issue concerns reflectance. Four-percent of light approaching an air/glass surface at near normal incidence will reflect back off that interface towards the source. This can cause countless problems, especially when power level measurements are central to an experiment, but it can also damage the laser source.

Back-reflected light can reenter the laser cavity and disrupt or permanently damage the equipment, so it is wise to add a safeguard against this occurence.

A polarizing beam splitter (PBS) is a device that can, as the name suggests, split a beam into its various polarization components before sending them in different directions. These are often designed to be cubic or rectangular, and Figure 2.15 illustrates some possible designs.

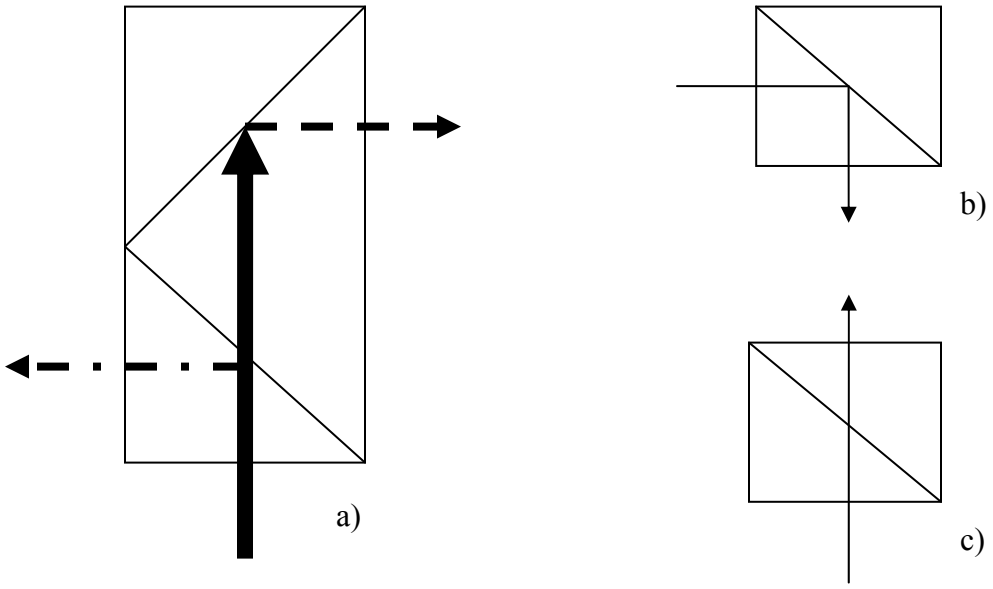

Figure 2.15. a) A PBS which divides the signal into two components. A PBS may also completely b) reflect or c) transmit light depending on the polarization. [10]

One key property of a PBS is its ability to select whether light will be reflected or transmited at the interface. If light linearly polarized in the x-direction is reflected at the interface in Figure 2.15b, then light linearly polarized in the y-direction would be transmitted at the same interface, as shown in Figure 2.15c. This selective reflectance and transmittance makes it possible to rid a system of unwanted signals, such as back reflections that can damage the laser source.

To review polarization theory, light is a wave with both a magnetic and electric component. A generic representation of light can be written:

$$\vec{E}(z,t) = \vec{E}_x(z,t) + \vec{E}_y(z,t) \tag{2.18}$$

$$\begin{aligned} \vec{E}_x(z,t) &= \hat{i}E_{0x}\cos(kz - \omega t) \\ \vec{E}_y(z,t) &= \hat{j}E_{0y}\cos(kz - \omega t + \varepsilon) \end{aligned} \tag{2.19}$$

where 2.18 shows light propagating along the z-axis is made up of an x and y component of the electric field. Equation 2.19 shows those components are periodic functions, and thus will oscillate like waves as time and distance, in z, are passed. The other variables are fairly self-explanatory, with *t* representing time, *k* being the propagation number based on wavelength, λ, such that

$$k = 2\pi / \lambda \tag{2.20}$$

and ω labeled the angular frequency which goes as

$$\omega = 2\pi / \tau = 2\pi v \tag{2.21}$$

with *v* as the wave's frequency and τ being the period. The relative phase difference, ε, will determine whether the x and y components are in or out of phase. Thus, if ε = 0 both components reach maximum magnitudes at the same time, and the light is classified as linearly polarized. Another type of light polarization is circular, where $\varepsilon = -\pi/2 \pm 2m\pi$ and *m* is any integer or zero. Whereas linearly polarized light appears as a wave oscillating in one plane, with the x and y components reaching their maximums and minimums at the same point in time, the two components of circular light are working out of phase. Figure 2.16 provides a visualization of a linearly polarized beam and a circular beam. The other type of light classification is elliptical, and this contains all the values of the relative phase difference other than zero or $\varepsilon = -\pi/2 \pm 2m\pi$.

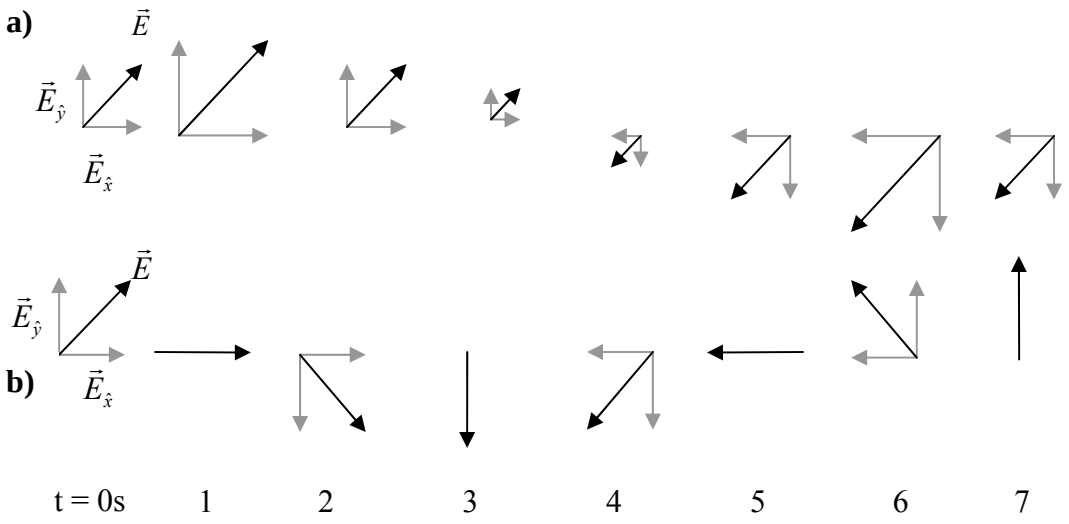

Figure 2.16. a) Linear polarized light and b) circularly polarized light.

Now that light polarization has been introduced, the challenge of ensuring the unwanted back-reflection is polarized in such a way to be filtered out in the PBS can be addressed. Wave plates and rhombs are optical devices that can alter the polarization of a wave by predetermined amounts. This is possible by slowing down one component of the E-field relative to the other. If the x-component in Figure 2.16a is slowed down with respect to the y-component by a particular amount, it could change to Figure 2.16b at t=1. In other words, while the components were initially in phase, the delay of the x-component saw the y-component change at a different rate; hence, a new polarization is achieved. This can be achieved with carefully designed crystals where the axes have different indices of refraction, and the exact amount of shift can be selected for any scenario. For the aforementioned task of filtering out unwanted reflections, if linear light enters a rhomb acting as a quarter-wave plate, circular light will exit. A quarter-wave plate adds a relative phase shift of a quarter-wave, $\lambda/4$ or $\pi/2$. The ingenious part of this design is that any Fresnel reflection after the rhomb will be circularly polarized but

with rotation in the opposite direction. As the reflected light passes back through the rhomb it attains another $\lambda/4$ shift. Thus, it is now linearly polarized orthogonal to the original state and will pass directly through the PBS, as seen in Figure 2.15c. This combination of a PBS and a quarter-wave plate is therefore an extremely beneficial safety measure to add to any optics-based experiement.

III. Experimental Methods and Equipment

Chapter III presents the methods and equipment used to examine the feasibility of alkali-filled, hollow-core fibers contributing to collision broadening. First, an overview of the many components to this experiment will be provided. Each individual piece of equipment, or relevant grouping of equipment, will then be discussed in greater detail.

3.1 Equipment Overview

The complexity of this experiment is apparent when the necessary equipment is listed in its entirety. Figure 3.1 is a basic schematic that illustrates the order and variety of the equipment used. The Velocity tunable diode laser starts the experiment, as its beam propagates through the polarizing beam-splitter and the quarter-waveplate, as mentioned in Section 2.3. The beam, which is initially elliptically shaped, is altered in the cylindrical telescope. A new circularly shaped beam passes through a chopper, a piece of equipment that changes the signal into a periodic pulse, and into a beam-expanding telescope. Directional mirrors help to guide the beam through a microscope slide, which picks off 4% of the signal due to Fresnel reflection, while the rest of the power proceeds into a periscope, a necessary addition given the design of the glass mounts used in this experiment. The beam enters the 10x microscope objective and is focused down for coupling into the fiber, which is encased in the glass mount. The light is propagated through the HCF, theoretically interacting with the Cs and He that are in the mount and the core of the fiber. The other end of the fiber is also enclosed in a mount, though this side only provides a vacuum as opposed to any gases. The light exits the fiber and the mount shortly thereafter, finally being measured by the power detector. Meanwhile, the 4% that was picked off with the microscope slide is guided through the lower portion of

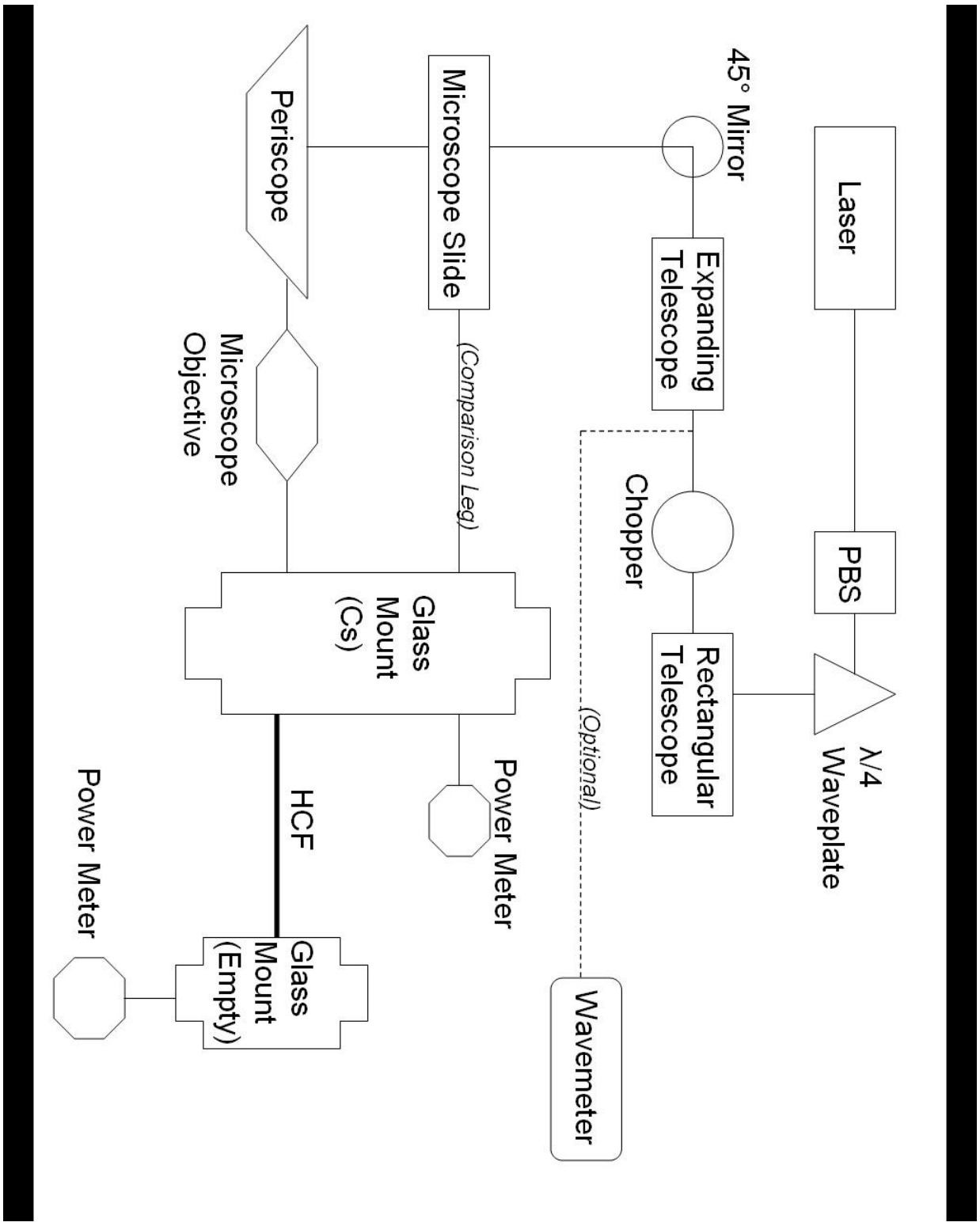

Figure 3.1. Entire HCF Cs Experiment Setup. All optics were either uncoated or coated specifically to include 848-854nm.

the mount, which also includes Cs. This allows for an identical pressure and chemical environment in which to measure the non-fiber absorption spectrum. In other words, this comparison leg provides a baseline which can be judged in relation to whatever results the fiber leg generates. Finally, a pop-up mirror can be used immediately before the beam-expanding telescope to redirect the beam into a wavemeter. This piece of equipment can offer a more precise measurement of the actual wavelength of the laser beam.

3.2 Tunable Diode Laser

The heart that pumps the entire experiment is the New Focus Velocity tunable diode laser, shown in Figure 3.2. The actual laser is the 6316 model while the controller is the 6300. The wavelength range is 848nm-854nm, with a published maximum output of 100mW, though the beam accuracy and stability drops significantly as power levels exceed 25mW.

Basic operation of the laser is relatively straightforward. Once all of the connections are hooked up and the power is on, the user can set the center wavelength using the “track” button and the “wavelength adjust” knob. When setting the wavelength, the controller displays up to two decimal places, though only one decimal place accuracy is guaranteed. For example, scrolling to 854nm will show 854.00nm, but in steady beam operation only 854.0nm is certain. The other main reason for using this laser concerns the ability to wavelength scan over a preset range. The user can set the start and stop wavelengths, along with the desired scan speed, both up and down the range. This seemed to be particularly useful for our application, as we were looking for an absorption dip at a specific wavelength, all relative to the power level at the other wavelengths. The

only problem is that the standard scan for this laser did not appear to meet the requirements of this experiment. In initial tests, the scan was not progressing steadily through the range of wavelengths. Rather, it appeared to be a step function, a signal that would make seeing an absorption dip almost impossible. The solution to this problem added a few more pieces of equipment, though they are all basically assisting in getting the input setup correctly.

Figure 3.2. The New Focus Velocity diode laser operates through a range of 848nm to 854nm. It was mounted above the table to alleviate the need for multiple periscopes.

A Wavetek 12 MHz Synthesizer Function Generator, model 23, was used to generate a much more suitable wavelength scan. The New Focus controller allows for a BNC input for outside fine-frequency control. The function generator sends a periodic signal to the laser controller, which uses this signal to manage the piezoelectric transducer (PZT). The PZT applies a voltage to a small crystal which is attached to a mirror in the laser. The crystal changes in length based on the voltage level, thus moving

the mirror. The mirror in turn changes the nature of the laser cavity, which modifies the wavelength of the generated beam. This model applies a voltage in the range of ±3V to change the frequency by ±30GHz. In other words, the function generator's signal finely adjusts the generated beam, thus allowing for a smooth, steady scan over a chosen range.

The other consideration already mentioned above is the concern for accurate wavelength readout. If a scan is being performed centered on what appears to be 851.5nm, but is actually 851.6nm, that can mean all the difference in whether an absorption line is seen at the expected location, let alone even seen at all. A flip-up mirror, placed before the beam-expanding telescope, guides the beam into a wavemeter, specifically the Burleigh WA-10. A wavemeter is used to precisely measure the wavelength of a continuous laser beam. The WA-10 has some general adjustment controls, such as an expected wavelength range knob to give the equipment a rough estimate of where to start and an attenuator slot to control the amount of power allowed into the measurement cavity. A 1.0mW He-Ne guide beam is used to align the input beam properly, as this is critical for accurate use. Where the laser controller can, at best, read out to two decimal places, the Burleigh wavemeter can give a result accurate to five decimal places with certainty. This tool helps ensure a scan is being run over the exact range that is desired.

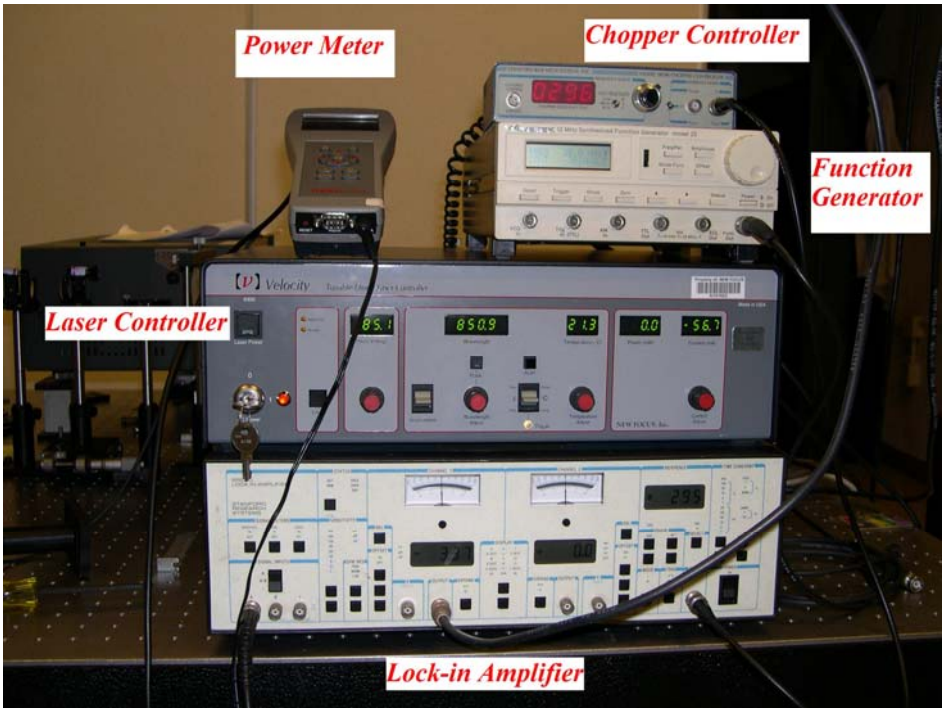

Figure 3.3. The control center included all components necessary to create the desired input signal as well as the tools used for accurate measurement and manipulation of the output signal. Not pictured: Oscilloscope and wavemeter.

3.3 Optics

The focus now shifts to the numerous optical methods and equipment that make the laser's signal usable for our application. Since the general concepts were addressed in Chapter 2, we can delve into the specifics surrounding actual pieces of equipment. All optics are made by New Focus, unless specified otherwise, and either uncoated or coated specifically to include 848-854nm.

The first optical devices are a polarizing beam-splitter (PBS) and a quarter-waveplate. The PBS is a small, glass cube measuring 2cm on each side, as seen in Figure 3.4. Upon initial placement in the beam's path, one must be extremely cautious to avoid damaging the laser due to Fresnel back reflection. At each interface a percentage of the

power will be reflected back in the direction of the laser. By placing the PBS so that the beam and the front interface form a 45 degree angle, we find the back reflection directed wide of the laser cavity. Then, returning the interface to a near normal incidence, we can follow the back reflection until it is set directly outside of the cavity hole. This setup allows for the closest to normal incidence without the back reflection actually reentering the laser, thus protecting the laser. The quarter waveplate is then placed directly after the PBS, changing the linear polarization to circular polarization. This particular quarter waveplate is a Fresnel rhomb, also seen in Figure 3.4, made of glass and measuring 1cm at the base and 3cm in height. A slight vertical and horizontal shift occurs upon propagation through the rhomb, but it is only on the order of a centimeter. The rhomb's 45° angle orientation converts linearly polarized light to circularly polarized light.

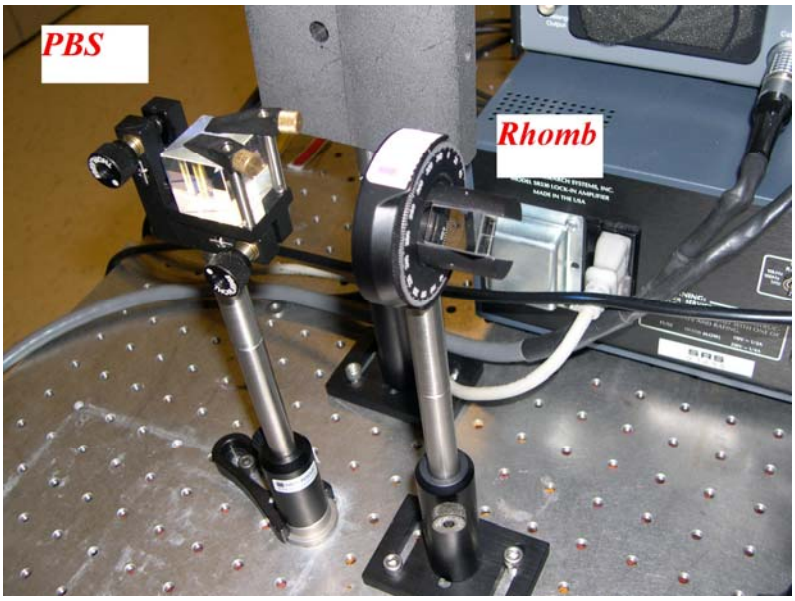

Figure 3.4. A polarizing beam splitter and a rhomb, acting as a quarter waveplate, protect the laser against damaging back reflection.

The next stage of the experiment deals with modifying the beam in efforts to improve beam quality and ease the expected difficulty of later stages. In order to

implement the next optical systems, it was necessary to master the ability to measure laser beam width. One significant and useful trait of our laser is that it produces a Gaussian beam. Although a beam spreads out uniformly on each side and can appear fairly wide, the actual beam width is measured to be where the majority of the power is located. The standard way to find this value is to first measure the total beam power. Then, by passing a razor blade edge across the beam's path, the points where 86.5% and 13.5% of the overall power are recorded mark the boundaries. In other words, the actual beam is contained inside those power boundaries. The measurement is taken on a micrometer which is attached to the razor blade, permitting very precise adjustments.

It is necessary to measure beam width along both axes, since some beams, including the one here, may not be circular. The height was measured to be 0.57mm while the width was 1.40mm. This would not always be an issue, but the desire to limit any additional factors that would contribute to the challenge of coupling into a very small fiber suggested an earlier fix. The solution was a cylindrical telescope, which expands only one axis of a beam; therefore, an elliptical beam with an elongated horizontal axis can be transformed into a completely circular beam, with equal length axes. Unfortunately, the perfect theoretical solution may not always be attainable in the laboratory. Designing a cylindrical telescope with the lenses available presented us with a choice between two less-than-optimal setups: a 2x or a 3x telescope. Mathematically, we would have preferred a telescope with a 2.4x magnification along the vertical axis, but this was impossible given the available lenses. Hence, we chose the 2x calculating that a 1.14mm beam is better than a 1.71mm beam when compared to our steady axis measurement of 1.40mm. The focal lengths of -100mm and 200mm required a 100mm

distance between the two lenses, and can be seen in Figure 3.5. The final result was a beam that was still technically elliptical, but much more circular than the original.

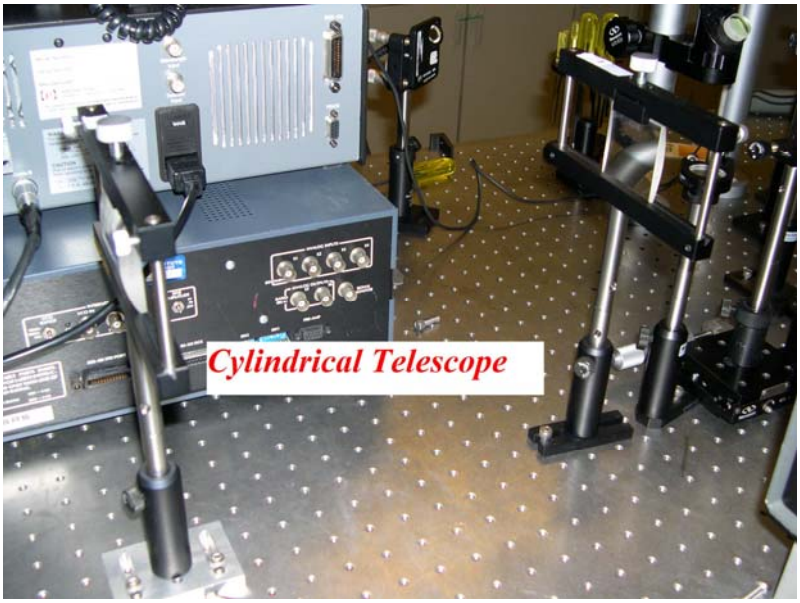

Figure 3.5. A cylindrical telescope was implemented to reduce the coupling issues from an elliptical beam.

Another decision heavily influenced by the thinking-ahead strategy was to add a beam expanding telescope. More specifics about the glass mount will be addressed in the next section, but the point that is relevant presently is the concern for how much distance we had to work with between the fiber tip and the microscope objective. This estimate of 13mm on the initial schematics combined with the limits of available objectives led us to choose a 10x microscope objective. A 10x objective has a focal length of around 15mm and a working distance of 13mm, which is simply the distance between the physical end of the objective, as opposed to the back principle plane, and the focus. Using this focal length and Equation 2.15, along with the published HCF NA of 0.20, one can calculate a beam width of 6.1mm. This immediately caused a change in plans, as the microscope objective's diameter was only 5mm, and passing a beam that wide through the objective would yield significant clipping. Thus, a concession was made and we decided to use the

standard 10x microscope objective with the largest beam that would make it through the objective unclipped. The rationalization for this decision was founded in the theory and Equation 2.15, since undershooting the beam width still met the NA coupling requirements, while a wider beam width would require a larger angle and may not be coupled successfully. The downside to this decision was that we did not optimize the mode size, a factor that may have affected our coupling success.

We finally settled on a 3.54x beam expanding telescope, using lenses of focal lengths -25mm and 88.5mm. After placing the two lenses 53.5mm apart and adjusting for height differences in the mounts, the final output beam was 4.96mm in width and 4.04mm in height. Once again, this was not the ideal beam size or quality, but given our ever increasing balancing act of factors and considerations it was the best we could do with the tools at hand.

The next optical stage concerns the creation of a comparison leg and simple beam guidance issues. A comparison leg was desired to make simultaneous measurements of an ordinary Cs absorption line to view side by side with whatever results were generated from the fiber leg. It would have been very simple to use another pop-up mirror, like the one used with the wavemeter, but then the simultaneous requirement would not be met as the beam would be completely redirected. Instead, a thin microscope slide cover, between 0.13mm and 0.17mm thick, was placed in the beam's path and angled so that the Fresnel reflection made up of 4% of the power could be redirected. Thus, the same back reflection that was the reason for more caution early on can now be used to our advantage. Since the microscope cover slip is so thin, the 0.15mm between the interfaces made it possible to measure both reflections on the same detector. This gave us twice the

power level, or 8% picked off for the comparison leg, which translated to higher, more easily detectable absorption levels.

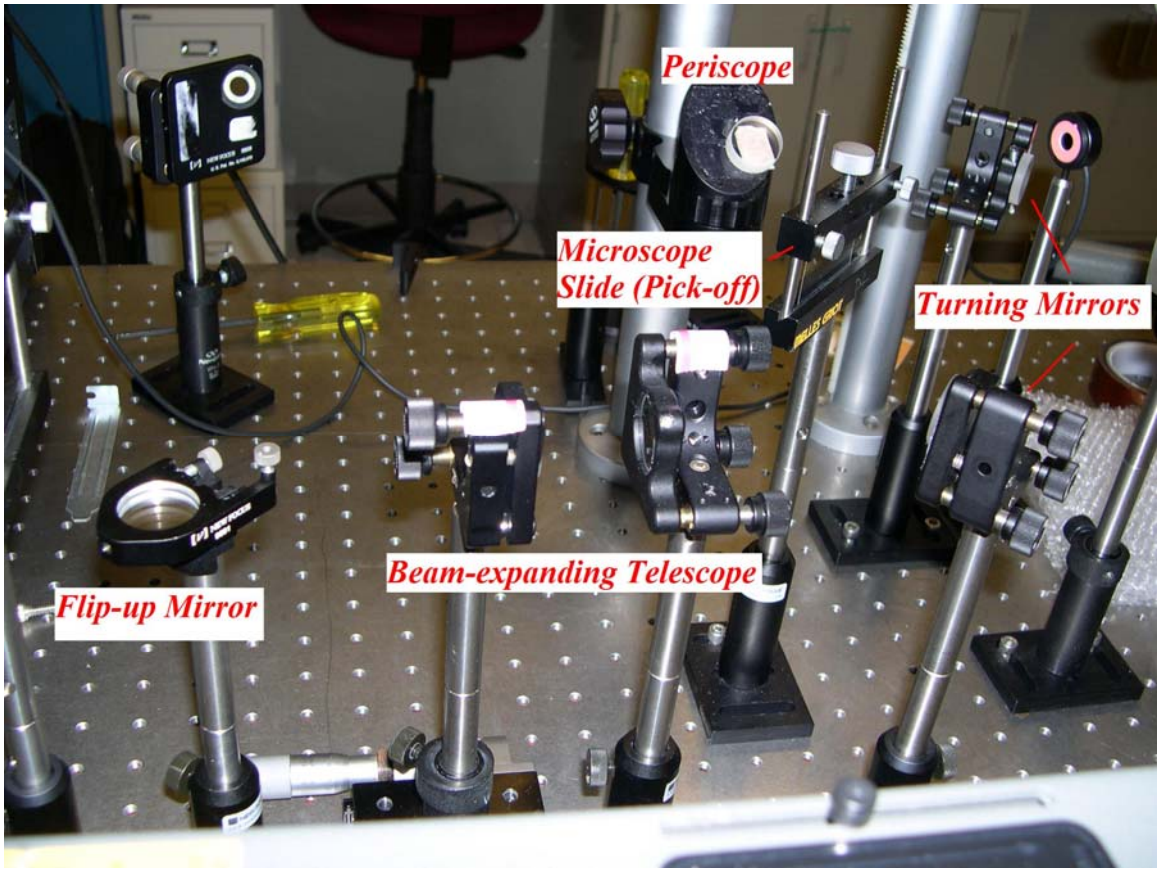

Figure 3.6. The optics table became increasingly crowded as the input beam was expanded two different times, turned, and vertically displaced. The microscope slide took advantage of the Fresnel reflections to create the comparison leg's signal.

The beam power that did not get redirected for the comparison leg was intended for coupling into the fiber, but in order to do this it had to be translated about 10 inches up due to our glass mount design. We accomplished this task by implementing a periscope, using two mirrors at 45 degree angles to first reflect the beam straight up and then horizontal yet again; only 10 inches higher off the table. Both this leg's mirrors and the mirrors used in directing the comparison leg were either silvered for general reflection or coated specifically to include the 848nm-854nm range of our laser. The

silvered mirrors were not optimal, but they were only used when we ran out of the properly coated mirrors, the latter of which provide over 99.5% reflection at 45 degrees according to the manufacturer, New Focus.

The last optical component is the 10x microscope objective, which has already been discussed in detail where the decision criteria are concerned. It is worthwhile, however, to mention some of the other setup challenges. In order to couple light into a fiber, it is imperative to have as much control over the fiber location or the objective location, though control over both would be ideal. In this experiment, the fiber was held immobile, meaning the control had to be entirely in the objective setup. This would appear very straightforward at first, seeing as how there are plenty of fairly precise microscope objective mounts that provide adjustment along every axes, but our mount was designed and built before we really understood the challenges it would present when combined with the microscope equipment at hand. Namely, some valves and connections for the vacuum system which were attached to the mounts made it almost impossible to get the objective in place where it could have a chance of being adjusted for successful coupling. Eventually, we attached the objective to the side of a mount and oriented that mount sideways, rotated 90 degrees from its intended orientation. This allowed us to get the objective in position for coupling while avoiding the various valves. The beam, upon exiting the periscope, passed directly through the objective holder, which is just a barrel, and roughly onto the fiber tip. This approach put the beam in the general location before the objective was attached, giving us a closer starting point to the best coupling position.

3.4 Glass Mounts and Fiber

The most elaborate component in the entire experiment was the custom designed and built glass mounts. The motivation behind the mounts was two-fold: hold the fiber and contain the cesium. All of the basic fiber-objective mounts in the labs are designed for generic fibers, not hollow-core fibers filled with a very reactive gas. So, we set out to design a mount that would satisfy all of our requirements. First, the fiber needed to be held completely in place with an air-tight seal. This ensures better coupling potential and contains the harmful cesium inside the mount or fiber at all times. There was also a desire to add a vacuum pump and buffer gas to the system, theoretically facilitating in the cesium diffusing down the fiber core, which called for ½ inch openings where connections could be made. Lastly, in order to have the best chance of coupling into the fiber we needed a clear, flat portion of glass directly in front of the fiber tip. This would limit the amount of unwanted aberrations while maintaining beam quality.

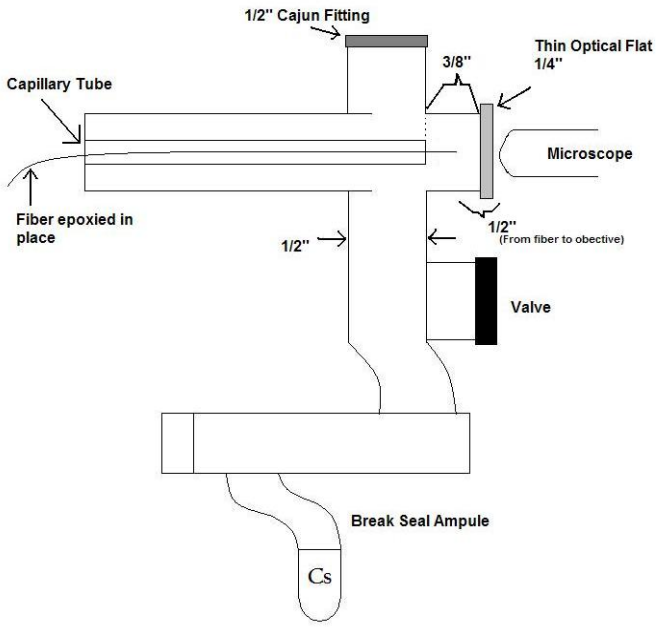

Figure 3.7. The initial mount schematic. The biggest change in the final design was an additional port for a vacuum attachment.

Considering this long list of requirements, it was fortunate that we were able to utilize the skills of a professional glass blower to combine all of the individual components together into one solid mount. We decided to go with two different mount designs, as seen in Figures 3.8a and 3.8b, since we needed to contain the fibers at both ends but only one end would contain the cesium. The more complex design contains a cesium break seal ampoule fused onto the bottom, a small piece of metal being used to break the seal and release the cesium when opportune. Above that, a valve was used for isolating the cesium source from the main cavity even after the seal was broken. The main cavity contained two ½ inch tubes, one connected to the vacuum system and the other to the buffer gas. The larger cavity was also fused to a small, 1/4 inch glass capillary tube, whose small hollow core holds the fiber in place. This capillary tube extends from the main cavity about 2 inches, just enough to allow for fiber positioning before the fiber was finally glued in place. The other mount was almost identical, save for the absence of the cesium and valve. Early discussions entertained the idea of attempting to have cesium diffuse from both ends, but this idea was deferred for simplicity's sake.

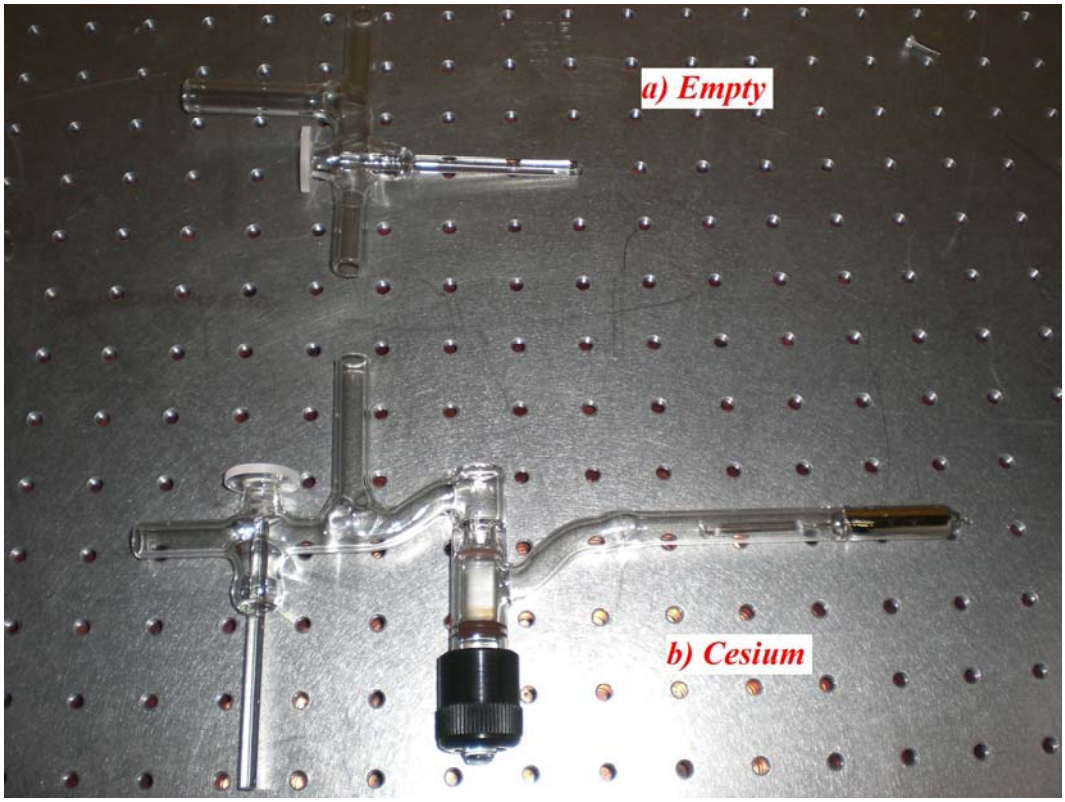

Figure 3.8. a) The basic mount used at the vacuum side of the setup. b) The cesium mount was more elaborate, taking the basic mount and adding a valve and the break-seal ampoule.

The vacuum system for this experiment was added to assist in the cesium's progress down the fiber core. An Alcatel Pascal Series 2015 C2 pump was chosen, partially due to its availability and partially due to the C2 classification, which translates to the option of using Fomblin oil instead of typical pump oil. Fomblin oil was chosen because of its inert nature, which was attractive given the possibility of the very reactive cesium making its way into the pump. The pump was hooked up with ¼ inch steel tubing, which was easily bent to fit around the rest of the equipment on the lab table. Quarter-to-half inch Cajun fittings were made from the steel tubing to the ½ inch glass on the mounts.

The other gaseous addition to the experiment came in the form of helium buffer gas. The concept behind the buffer gas was to have some other gas in the mount be pulled by the vacuum or diffuse with the cesium along the fiber core. Helium was chosen due to its availability and safe nature when mixed with cesium. The same Cajun fittings and ½ inch tubing were used to hook up the helium source tank to the cesium mount. The only other connections were between generic test tubes and the extra ports on the cesium-less mount, merely to finish closing off the system.

The hollow core fiber used in this experiment was the HC-800-02 manufactured by Crystal Fibre, as seen in Figure 3.10. The biggest factors in choosing this fiber for our experiment were obviously the hollow core nature and guiding based on the photonic band gap approach, allowing us to theoretically fill the fiber with gas, in our case cesium, but it was also the best option for our wavelength since its center operating wavelength is 840nm. The maker stresses some other key features of this fiber, including that 95% of the power propagates through the hollow core or the surrounding cladding holes. This is an attractive feature because most light that is coupled into the glass coating of any fiber will escape as it makes its way down the fiber. This dispersion and loss rate were not too much of a concern for our experiment, considering we were working with a meter or less of fiber. Additionally, this fiber had minimal Fresnel reflection, which was nice even though it was not crucial at this point given our earlier design considerations.

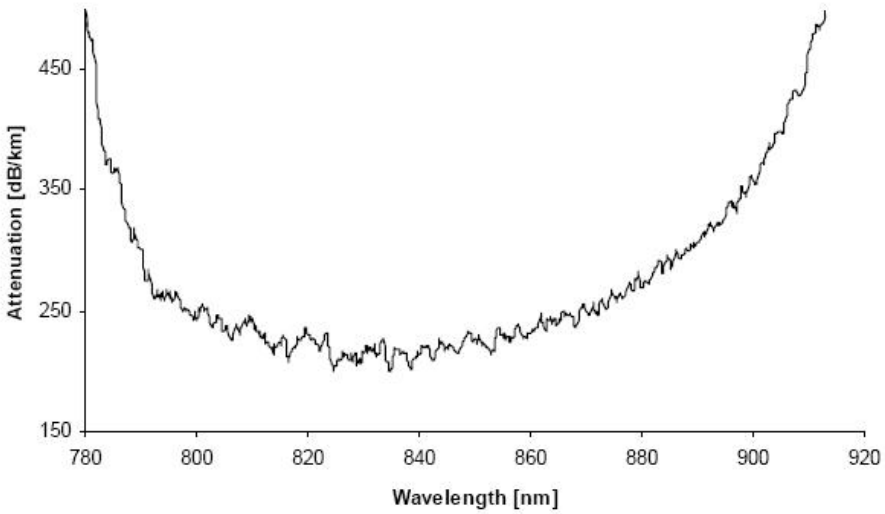

Figure 3.9. The HC-800-02 was the best option for an affordable, hollow-core fiber which would perform well over the wavelength range of 848nm-854nm. [2]

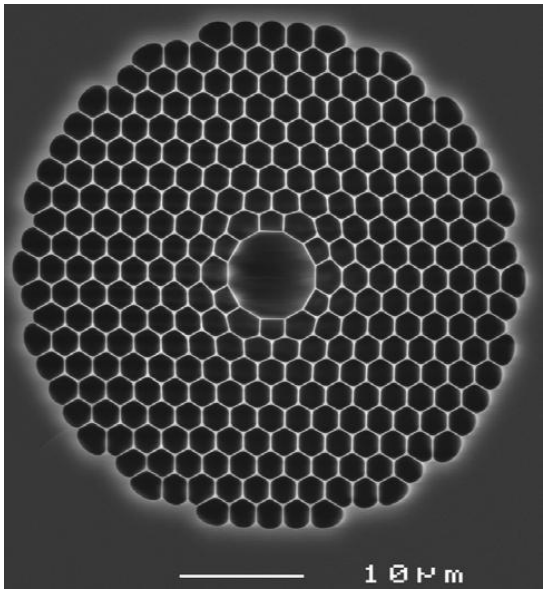

Figure 3.10. A close-up of the fiber highlights the hollow core and cladding holes, all of which could potentially contain cesium. [2]

Coupling light can be a challenge with any fiber, but our HCF had a core diameter of 6.8 microns; consequently, preparing the fiber was even more critical to avoid coupling difficulties. The tips of a fiber should be as clean as possible, giving the signal a clear window into the core. This fiber is made with a polymer coating which protects its

signal from the environment, but this coating must be removed with a stripper that works a lot like an electrical wire stripper, just on a much smaller scale. The fiber is then placed in a cleaver which is used to "cut" off a portion of the stripped end. Many cleaving options were available, but we found the 3SAE Technologies LDF rotary cleaver the easiest and most reliable. The cleaver does not actually slice or cut the fiber; rather it nicks one edge, twists the fiber, and then pulls it apart. The nick should be enough of a defect to cause the fiber to break exactly at that point. The concept is akin to the serrated edges on candy bar wrappers, which permit a clean tear instead of the less-than-elegant stretching and ripping. Despite the frustrations this fiber caused, which will be fully addressed in the next chapter, the cleaving process was extremely forgiving. Almost every cleave with either the automatic cleaver mentioned or a manual hand cleaver, manufactured by T&B, provided a near-perfect tip when observed under a magnifying viewer. This is probably the result of the hollow-core nature, since most of the surface is actually air and is completely unaffected by the cleaving process. Traditional fibers often require multiple cleaves or fiber polishing equipment to get a superior quality tip. Thankfully, our fiber did not require this level of preparation.

Once the fiber was prepared at both ends, we had to place it in the mount without damaging it. This meant feeding the fiber through the capillary tube and applying glue to the exposed end, sliding the fiber back and forth to work the glue at least a centimeter into the tube to guarantee a solid seal. We used Hardman's Double/Bubble epoxy, which is fast curing and experiences almost no out gassing. Once the epoxy was applied and the fiber tip was within a centimeter or so of the glass window, we allowed it to fully cure. We repeated this same process on the other side, which was extra worrisome seeing as if

we damaged that end we had already committed to the first side's finality. Before either side of the fiber was epoxied in place, we fed it through a ¼ inch copper tube which provided both protection and a medium for heat conduction around the fiber. Although we did not expect cesium to make it far into the fiber, in the off chance that it did we needed to keep the fiber warm so that the cesium wouldn't condense inside, completely blocking the signal.

In order to keep the mounts and the copper tubing warm enough to ensure cesium remained in its liquid and gaseous forms during data acquisition, we used two Staco Energy Products Co. Adjust-a-Volt's, which are merely variable autotransformers, along with some heat tape. The heat tape used was made up of woven cloth covering wires that give off varying amounts of heat based on the autotransformer's setting. We wrapped this heat tape around the glass mount, being careful to leave enough of a gap to get our beam through the comparison section and the glass flat in front of the fiber tip, as well as down the length of the copper tube. One strand of heat tape was used to cover the cesium mount while a separate strand covered the copper tubing. The rationale behind this strategy was based in the desire to keep the fiber warmer than the mount, making certain that no condensation occurred in the fiber and potentially assisting the cesium gas down the fiber.

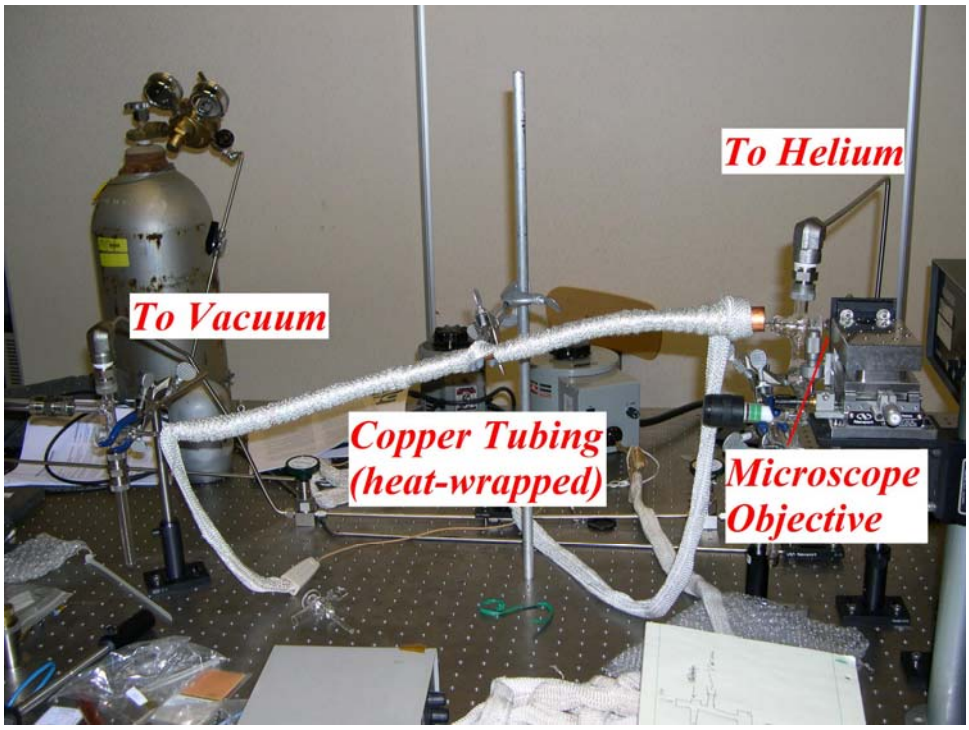

Figure 3.11. The fiber, contained in a copper tube wrapped in heat tape, spanned the two mounts, one of which was kept at a vacuum while the other contained cesium and helium.

The methods used to couple light into a fiber were varied, as were the levels of success yielded from each attempt. The methodical approach involved setting the distance between the microscope objective and the tip of the fiber slightly farther than the expected focal length and then working in. With each small adjustment in the z towards the mount, both the x and y were also adjusted until the maximum power output was measured at the other end of the fiber; the power measurement equipment will be addressed in the next section. One thing we looked for when coupling was the amount of light escaping from the first few inches of the fiber. Since this was not easily quantifiable, other than how it affected the power measured at the other end of the fiber, we basically used an infrared viewer (IR viewer) and watched how the fiber's glow changed in relation to the power output. If the majority of light was making it into the core, then very

minimal light was seen coming out of the fiber coating. If the fiber appeared to glow then the light was not going into the core, but rather into some combination of core, cladding, and coating. If we were to make a peak-and-valley analogy, a peak of escaping light meant the light was coupled into the glass coating. A valley, on the other hand, meant that the light was either being coupled into the core or not being coupled at all. The only way to distinguish between the two was to combine the clues attained from the IR viewer with the measured power levels, all the while adjusting the objective's position. Obviously, one can go for broke and quickly tweak the various knobs and hope for the best, and while this may work with some multi-mode fibers which typically have a larger core, the likelihood of getting that lucky with a HCF with a mode diameter of 5 microns is slim-to-none.

3.5 Measurement Equipment

Any experiment is only as good as the measurement tools employed, so it is no wonder that we should speak to the many machines that assist in the data acquisition process. The Burleigh wavemeter was already discussed in the laser section, so we'll start with the power meters.

In order to measure the amount of light successfully coupled through the fiber, as well as comparison power levels at various points throughout the optical chain, we employed two different power meters. The first was a Thorlabs S122B which worked well for steady power measurements. Setting the readout level for the expected power level and desired decimal output, as well as specifying the operating wavelength, was extremely straightforward. Unfortunately, this power meter did not seem to respond fast enough when we began scanning across a wavelength range. At this point, we switched to

a silicon detector produced by Edmund Optics. When tested against various scan speeds, the Edmund detector responded and displayed the data at an adequate resolution.

The only concern when using either of these power meters was the accuracy of the readout due to the poor beam quality incident on the detector. For example, when propagating through the comparison leg, the light passed through a test tube, not an optically clear glass flat. This caused the beam to spread out horizontally, often wider than the area of the detector. Depending on where we placed the detector we saw different power levels, obviously, but the fact of the matter was that some of the light that was making it through the glass was undetectable. Thankfully, this was not a major concern. We merely wanted to see a relative dip at a certain wavelength. Then again, this is considering that the dip would be uniform over the wide beam, making the portion that was being detected standard with the rest of the beam. Therefore, it is reasonable to assume that this divergence did not distort the qualitative measurements we sought in the comparison leg, and definitely had no effect on the fiber leg due to the glass flats.

The tool that helped us to discover that the Thorlabs detector would not meet requirements during the wavelength scan was a Lecroy LC584AM Oscilloscope (O-scope). Using a BNC cable to display the power level on the O-scope screen, we were able to zoom in and determine that the response time for the Thorlabs detector was not sufficient for our application. The O-scope substantiated this claim when we switched out the Thorlabs detector for the Edmund detector under the same conditions and successfully saw the absorption dip. We also used the O-scope to display the periodic function generated by the Wavetek function generator, discussed in Section 3.2. This was extremely helpful in troubleshooting and calibrating the laser scan, since we could see

where the dip was in relation to the function, and whether it was oscillating quickly near the ends of the function or if it was centered in the scan. Also, the O-scope had an option to average any input signal over multiple iterations. This was crucial in identifying the dip amongst all the noise, since the randomness of the noise was somewhat filtered out in the averaging, while the dip became more obvious with every pass.

Although the averaging function on the O-scope assisted in picking out the small trends in a signal, a lock-in amplifier combined with a chopper provided far superior small signal amplification. A chopper is a rotating disc with periodic slots, changing a continuous signal into a staccato signal, equally alternating transmission and blockage. We used a Stanford Research Systems Inc, model SR540 chopper and controller, and placed the chopper in the middle of the expanding telescope. This decision was based purely on ease of placement with regards to the rest of the lab design. The chopper's periodic signal would be worthless in itself, so we fed the chopper's rotation frequency into a lock-in amplifier, an SR530 also made by Stanford Research Systems Inc. Essentially, the lock-in took the power level from the detector and amplified the parts that corresponded to the holes in the chopper as determined by the chopper frequency. A signal could then be amplified at the points that we are actually concerned with, helping to eliminate some of the noise and uncontrollable oscillations inherent to the equipment being used. Thus, a small change in power level could be amplified and separated from noise.

IV. Results and Analysis

4.1 Results

Despite all the careful thought and work put into a project, sometimes things just do not turn out as planned. Regardless of intentions and expectations, we were able to gather worthwhile data that provided opportunities for substantial discussion.

First off, we accurately measured the cesium dip at 852.34nm, as seen in Figure 4.1. Using our comparison leg, we wrapped the heat tape in such a way to allow for a clear shot through the vertical test tube portion of the mount. After some adjustments to the lock-in and O-scope we finally saw the dip on the display, though we could easily see the scattering in the mount due to absorption and reemission.

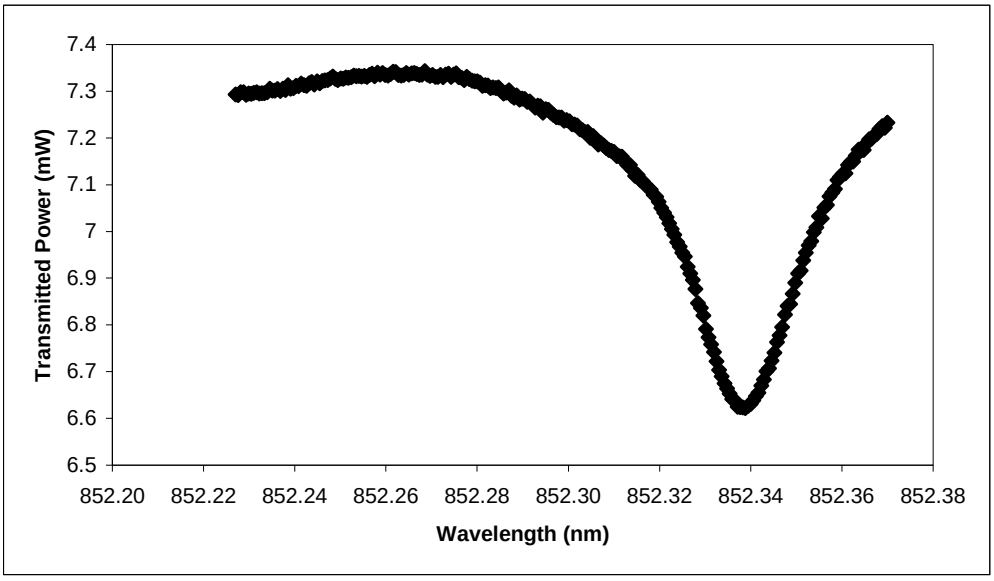

Figure 4.1. Cesium absorption. At standard atmospheric pressure a single absorption dip is visible at 852.34nm.

This piece of data was to be used as a baseline for comparison with regards to the data gathered from the fiber leg. Unfortunately, we never managed to get this to work as intended. After transmitting a workable amount of light through the fiber in

its final setup, excluding actually exposing the tip to cesium, we became concerned with the fluctuations in transmitted power, as seen in Figure 4.2.

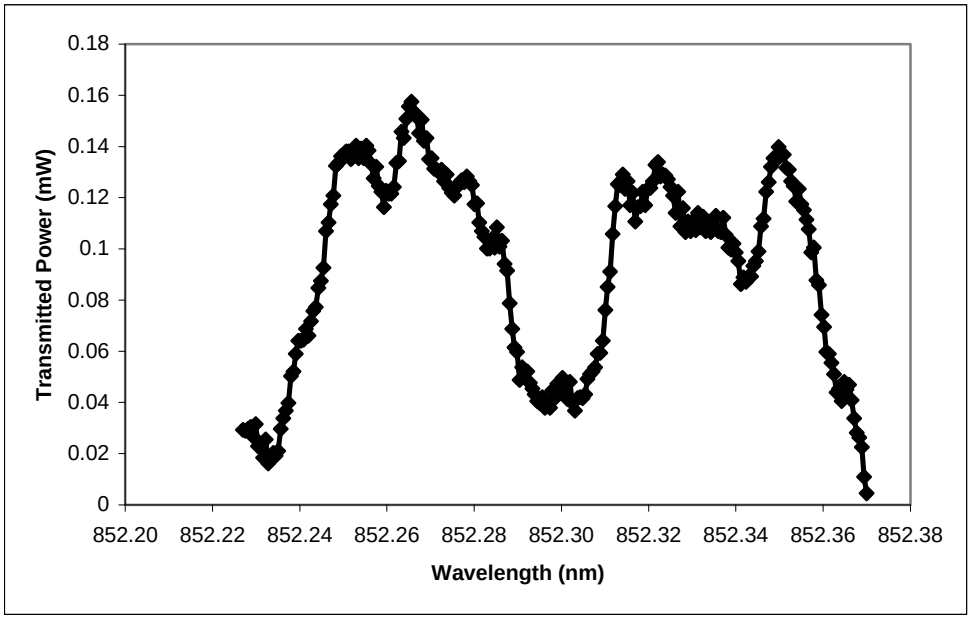

Figure 4.2. Fiber wavelength dependence. Even without a cesium presence, the fiber's transmitted power varied greatly.

This discovery, repeated numerous times with different power levels and scan speeds, forced us to investigate the cause of this fluctuation. Figure 4.3 demonstrates the power coming directly out of the laser during a typical scan and Figure 4.4 demonstrates the seemingly unrelated nature of the two measurements.

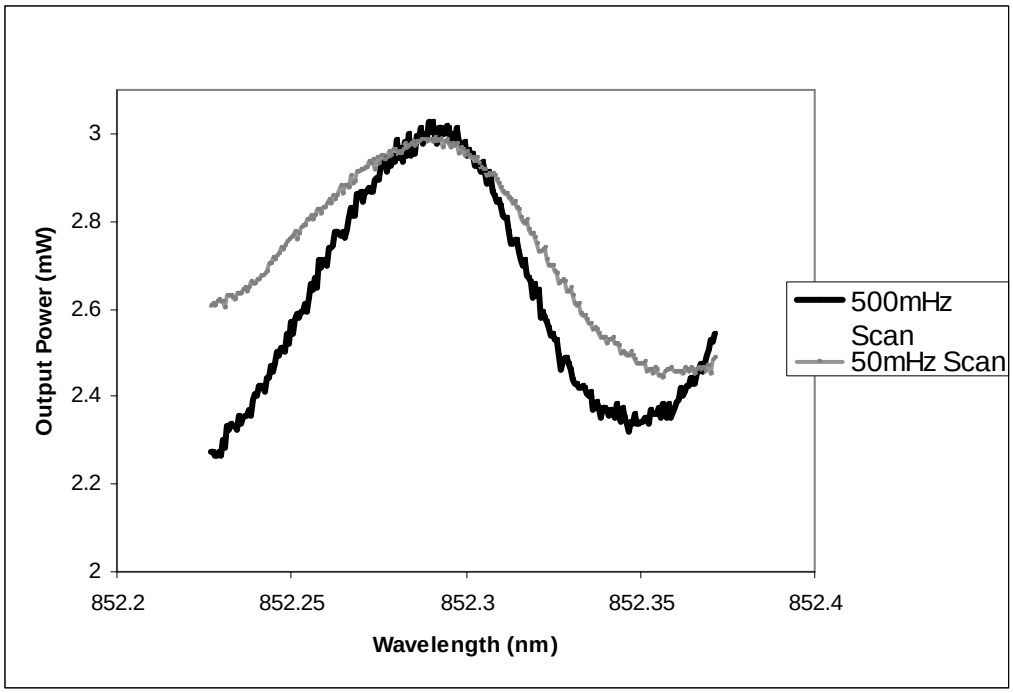

Figure 4.3. Laser source power variation. This data illustrates the unstable nature of our laser.

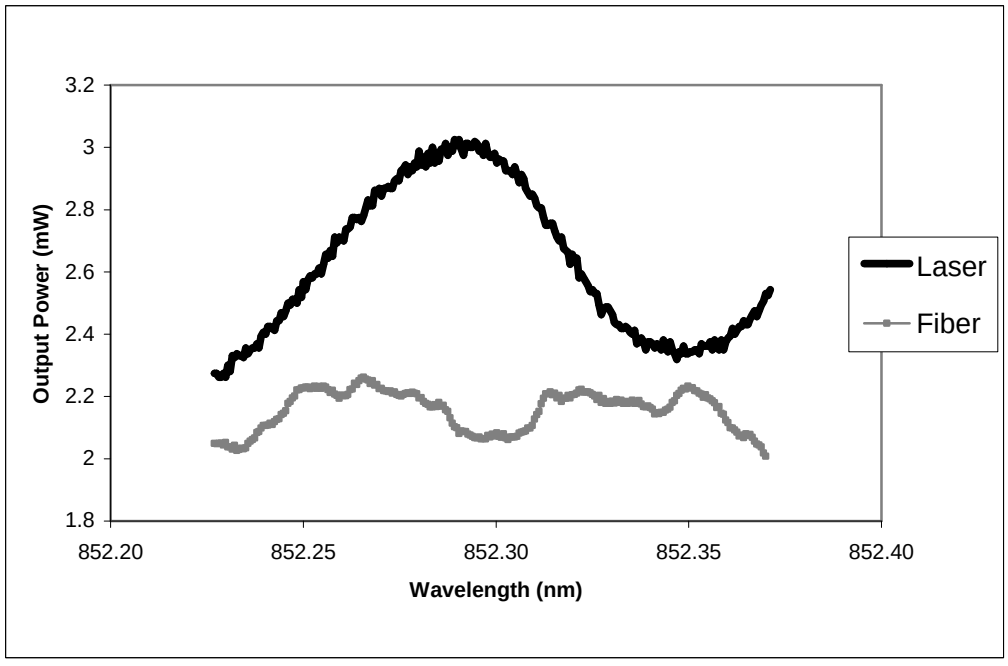

Figure 4.4. Laser and fiber scans. The variation of the source is not clearly related to the variation measured on the other end of the fiber. Fiber power shifted up by 2.0mW for display.

At this point, we knew the chance of attaining irrefutable evidence of collision broadening was small. However, with hopes that these fluctuations would form a predictable average over time we pressed on. Baseline scans were transmitted through the fiber using the function generator set to 50mHz and 500mHz, after which the fiber tip was finally exposed to the cesium. Identical scans, both in number of sweeps and input power, were performed and the results are shown along with the baseline data in Figure 4.5.

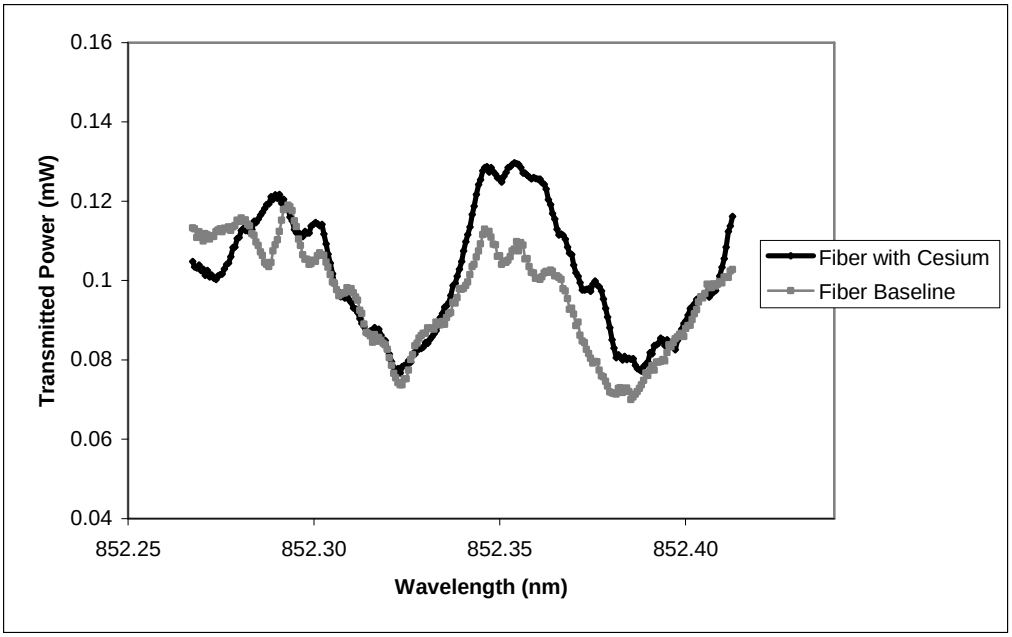

Figure 4.5. Cesium and baseline comparison. The variations are not simply shifted or altered in magnitude, but are clearly more random and unpredictable than hoped for.

Evaluations were made as to the possibility of manipulating the data in hopes of exposing the presence of a cesium absorption dip; however, all theories lacked enough promise to justify pursuit.

4.2 Analysis

Considering the nature of data presented in the previous section, it was prudent to reevaluate some of the assumptions and theory behind our intentions. First, however, it may prove equally helpful to discuss the various troubles that plagued this experiment and suggest remedies that may streamline future attempts.

Obviously there were plenty of issues to deal with in this project, but the most frustrating had to be the fact that almost every component was joined together. One major reason for this was due to the need to keep the cesium isolated from air and leaks. Cesium, as already pointed out, is very reactive when exposed to water. Thus, it was necessary to seal the entire system off to keep the cesium from reacting and becoming ineffective in the absorption task. If the cesium ampoule was somehow made removable and replaceable the entire design would be greatly simplified.

One reason the cesium implementation would be streamlined if made replaceable is due to the challenges presented by preparing and placing the fiber. After preparing the fiber to have excellently cleaved tips, we had to slide the fiber through the capillary tubing into the glass mount. Even in the perfect placement, there was always the chance that the fiber picked up dust or residue contained in the tube. Thus, there was no way to know exactly what condition the tip was in when it was in position. While it may have looked perfect before, the five centimeter journey through the capillary tube once again made the tip's quality questionable. If we did feel confident that it was in the best condition possible, given the situation, we would glue it in place. This go-for-broke approach meant that if anything went wrong we may have made the mount, fiber, or both worthless. If the fiber broke off then we still

had a piece of fiber glued into the capillary tube. This was not disastrous in itself, as we could cut off the capillary tube after the point where glue was holding the fiber in place, but you could only do that so many times before you ran out of capillary tube. The more significant point here is the fact that we had fiber glued in place where an element that, when released, may react if the system was not completely sealed off.

Consider two scenarios: first, if the fiber was glued in place and the cesium was released and then there was a leak, then the entire mount was useless. Second, if the fiber was glued in place and the cesium was released, but then the fiber breaks, the only way to fix the fiber was to cut the capillary tube; hence, the system was opened up and the cesium became contaminated. In view of these setbacks and the suggestion to make the cesium replaceable, it would be wise to make the fiber removable and replaceable as well. While the current setup does not allow for complete assurance that the tip is well-suited for coupling and does not allow for easy replacement, mainly due to the inclusion of epoxy in the plan, a new design is proposed that should alleviate many of these problems. If each fiber tip were glued into a two inch long piece of capillary tube, with an easily measured distance exposed, and then slid into a $1/8^{th}$-to-$1/4^{th}$ inch tubing connector it could be removed and examined at one's leisure. Breaking the fiber would simply mean that a new fiber would need to be prepared in the same fashion and slid into the connector, admittedly not an easy task, yet better than the alternatives of cutting or replacing the mount.

If we had initially designed the mounts to allow for the replacement of fiber and cesium we would have spent significantly less time fixing or completely

rebuilding the experiment. Obviously this would have allowed for potentially more progress and attempts at gathering more data.

Another proposed adjustment was the possibility of shortening the fiber length between the two mounts. The thought here was to assist the pressure gradient by using a shorter "straw."

$$u_{\max} = \frac{Ga^2}{4\mu} \tag{4.1}$$

$$G = \frac{P_1 - P_2}{l} \tag{4.2}$$

Equation 4.1 calculates the max flow velocity, $u_{\max}$, based on the pressure gradient G found with Equation 4.2, where a is the radius of the tube, P_1 and P_2 are the pressures at either side of the tube, l is the length of the tube, and μ is the viscosity of the gas or liquid flowing through the tube. [11] When assuming that we have a pressure difference of half an atmosphere, a fiber length of 78.5cm, and using the viscosity of the buffer gas helium to be $1.85\times10^{5}\ \frac{kg}{m\cdot s}$, we get a maximum velocity of $5.45\times10^{-12}\ \frac{m}{s}$. If we shortened the fiber length to 20mm, almost a quarter of the initial length, the maximum velocity goes up to $21.39\times10^{-12}\ \frac{m}{s}$. Under inspection, this should be obvious given that the velocity is inversely proportional to the length, but the main takeaway from this discussion is that the fiber length is almost a non-factor.

If we wanted to get better flow of cesium through the fiber core based on Equation 4.1, our only other option, other than changing the fiber length, is to get a fiber with a larger core diameter. This would be a quadratic increase, but the problem here is finding a fiber that has a larger core and still works for our wavelength range.

The maker of our fiber, Thorlabs, makes another fiber which is centered on 830nm. However, our wavelength is still in the reasonable range of operation where attenuation is concerned. More importantly, the core of this other fiber is almost twice as large, with a diameter of 9.2 microns. Unfortunately, combining both a change to diameter and fiber length, we only increase the velocity by a factor of eight and are still dealing with velocities in the Pico-range (meter/sec). If we jump to the other end of the spectrum, starting with a capillary tube instead of a fiber, we estimate flow on the order of 0.3mm/s for a tube length of 20mm and a radius of 1mm. This is much more practical and justifies using a vacuum system. Achieving respectable levels of cesium inside this capillary tube would only take a minute. This scenario obviously does away with the fiber optics side of the experiment, but it may be better to start large and progress smaller until the broadening is measurable.

The other possibilities for assisting the cesium through the core concern both the simple concept of diffusion and the more complex concept of radiation pressure. Estimating the contribution made by the laser in the form of radiation pressure is a complex task. In essence, we would like to get a very general idea of how much the laser is pushing the cesium down the fiber. To start, we would like to know how much momentum is transferred to each cesium atom per second as a result of the collisions with the incoming photons. This can be represented as

$$\beta(I)\cdot\hbar k \rightarrow \frac{kg\cdot m}{s^2} \tag{4.3}$$

where $\hbar$ is the reduced Planck constant, $k = \frac{2\pi}{\lambda}$ is the wave number, and $\beta(I)$ is a function of irradiance that yields the interactions per atom per second. Dividing by mass gives us

$$\frac{\beta(I)\cdot\hbar k}{m_{Cs}} \rightarrow \frac{m}{s^2} \tag{4.4}$$

which is an acceleration, where m_{Cs} is the mass of cesium. Finding the velocity of each atom per second requires integrating

$$v(t) = \int_0^t \frac{\beta(I)\cdot\hbar k}{m_{Cs}}\,dt = \frac{\beta(I)\cdot\hbar k}{m_{Cs}}\,t \tag{4.5}$$

where every variable should be familiar except for the time, *t*, which will be addressed later.

At this point we know *hk* based on our wavelength and the mass of cesium is a readily available value, but the *β(I)* term needs some explanation. We will need to find irradiance, which we know, in general, to be

$$I = \frac{P}{A} \tag{4.6}$$

where *P* is incident power and *A* is the area of exposure. By dividing this by the energy of each photon, *hv*, we arrive at a value giving us the number of photons per area per second. We want the number of interactions per second, thus giving us our *β(I)*

$$\frac{\#\,photons}{A\cdot\sec} A \rightarrow \frac{I}{hv}\sigma = \beta(I) \tag{4.7}$$

where σ is the absorption cross-section of cesium. This cross-section takes care of the area in the denominator since it is the area around a cesium atom that could actually absorb a photon. By plugging in our frequency, $3.52\cdot10^{14}\,Hz$, the cesium cross section, $2.83\cdot10^{-19}\,m^2$, and the max power in the fiber, 0.2mW, we calculated a *β(I)* of $2.4\cdot10^{15}\,\frac{photons}{\sec}$.

Combining Equations 4.7 and 4.5 gives us a usable function for velocity, but first there is a conceptual issue to tackle. The velocity, in its current form, would simply increase as a function of time until our cesium was speeding down the length of the fiber instantaneously. Clearly, the helium buffer gas or some other obstacle would slow the cesium's progress, but the question is by how much. If we assume that a cesium atom will collide with a helium atom and completely stop at an average time interval, said to be $t_{collision}$, then we can greatly simplify the problem. Now, we can find the average velocity

$$v_{avg} = \frac{1}{t_{collision}} \int_0^{t_{collision}} v(t)dt = \frac{1}{2}\frac{\beta(I)\cdot hk}{m_{Cs}} t_{collision} \tag{4.8}$$

which can be assumed to be the continual velocity of a cesium atom through the fiber. To get a rough estimate of what we should expect, we employed the value of $10^8 \frac{photons}{s}$ as our $\beta(I)$, which is the maximum value to expect for cesium given the A_{21} coefficient; thus, the $\beta(I)$ we calculated earlier would yield impossible results if used. The $t_{collision}$ value was assumed to be 0.15ns based on the mean free path of helium at standard conditions. [11] In the end we expect a collisional momentum change with a velocity of $0.1\frac{mm}{s}$. Therefore it should take hours for a single cesium atom to make it the entire length of the fiber.

The last possibility of cesium making it down the fiber core concerns basic diffusion, stating that a high concentration of an element will move to an area of lower concentration over time in order to equilibrate the system. If we take

$$\Gamma = D\frac{dn}{dz} \tag{4.9}$$

to be the flux of an element across an area, where D is a diffusion coefficient and $\frac{dn}{dz}$ is the change in number density over length, we can substitute to get

$$v = \frac{\Gamma}{n} = D\left(\frac{\frac{P}{kT} - 0}{l}\right)\frac{1}{n} \tag{4.10}$$

where P is the pressure of Cs, ½ atmosphere, k is Boltzmann's constant, T is the temperature, 300K, and l is the length of our fiber. [11] We know all of the variables save one, which we can calculate using

$$D = \frac{2}{3\pi}\frac{(\pi mkT)^{\frac{1}{2}}}{nm\pi d^2} \tag{4.11}$$

where d is the diameter of our fiber and n is the atom number density, found using the ideal gas law. For cesium, we calculate a diffusion coefficient of $1.4\times10^{-5}\ \frac{m^2}{s}$ and a final velocity of $1.87\times10^{-5}\ \frac{m}{s}$. It is clear that diffusion is not the most promising way to achieve a cesium presence in the fiber, but with an exposure time of days it may suffice.

Given that the theoretical estimates suggest that within days, if not hours, cesium should make its way down a significant portion of the fiber core leads to speculation as to why a dip was not observed. If we are to assume that the coupling was too unstable to generate a usable transmission signal, then the question arises as to where that instability originated. Figure 4.4 displays the quizzical nature of both the fiber transmission and the laser output, but without a clear correlation between the two measurement points. One possibility is that the laser's output power has wavelength dependence, where some error is introduced regardless of scan speed. Figure 4.6 illustrates the internal workings of our laser, begging the question of how

precise the tuning mirror and other components are in adjusting wavelength while not only maintaining a constant power output, but also keeping the beam aimed in the same exact direction.

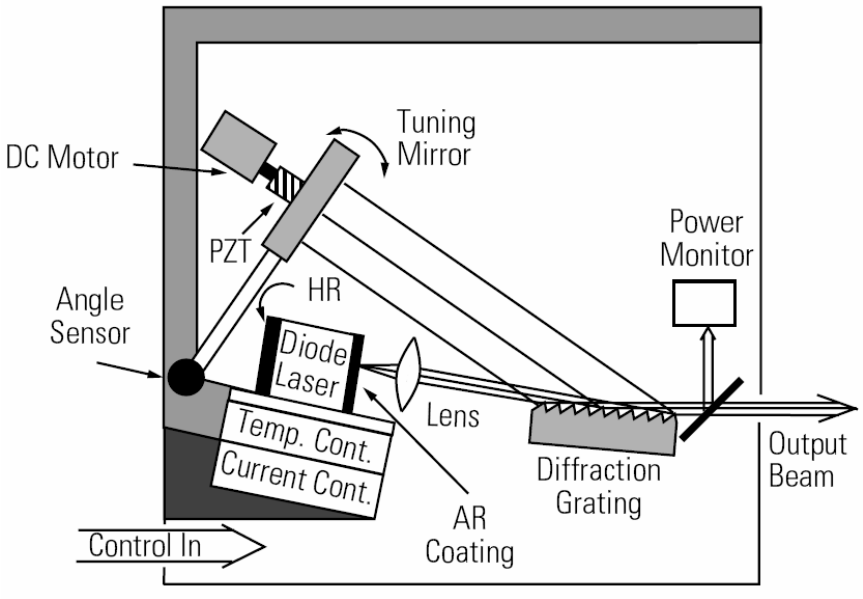

Figure 4.6. Laser cavity diagram. Any power fluctuation resulting from a wavelength scan could affect fiber transmission.

If one considers that we are dealing with a core diameter of only 6.8 microns, any wobble or shift of the beam during the scan could seriously impact the coupling efficiency. Various tests could be performed to determine if this is the case, including recording the spot location on a CCD video camera during a scan or using different aperture sizes in a power test during a scan.

Assuming that cesium did enter the fiber and that the recorded transmission levels are legitimate, one might ask if the lack of dip was due to the difference in conditions between the fiber leg and the comparison leg. There was definitely a possibility of some unforeseen variable changing and thus affecting our end result, but most of the conditions were identical. The entire mount was heated with the same strand of heat tape and was kept at a uniform pressure; therefore, the concentration

and vapor pressure of Cs was constant throughout the mount. This makes the fact that we did not even see a dip from the Cs in front of the fiber tip all the more curious. One variable that we did not initially have a concrete estimate for was the amount of collision broadening that could occur in the fiber. If the walls caused a significant amount of broadening then we could have overlooked a broadened dip as fluctuation in the fiber transmission or laser source. This is extremely unlikely considering that there was no semblance of a dip or even a relative minimum in the fiber transmission centered at the dip location. No amount of broadening could have actually shifted the dip's position. Also, the walls, acting as the broadening mechanism inside the fiber, were still much wider than the mean free path of helium, 168nm, which was an indicator of the pressure broadening seen in the comparison leg. [11]

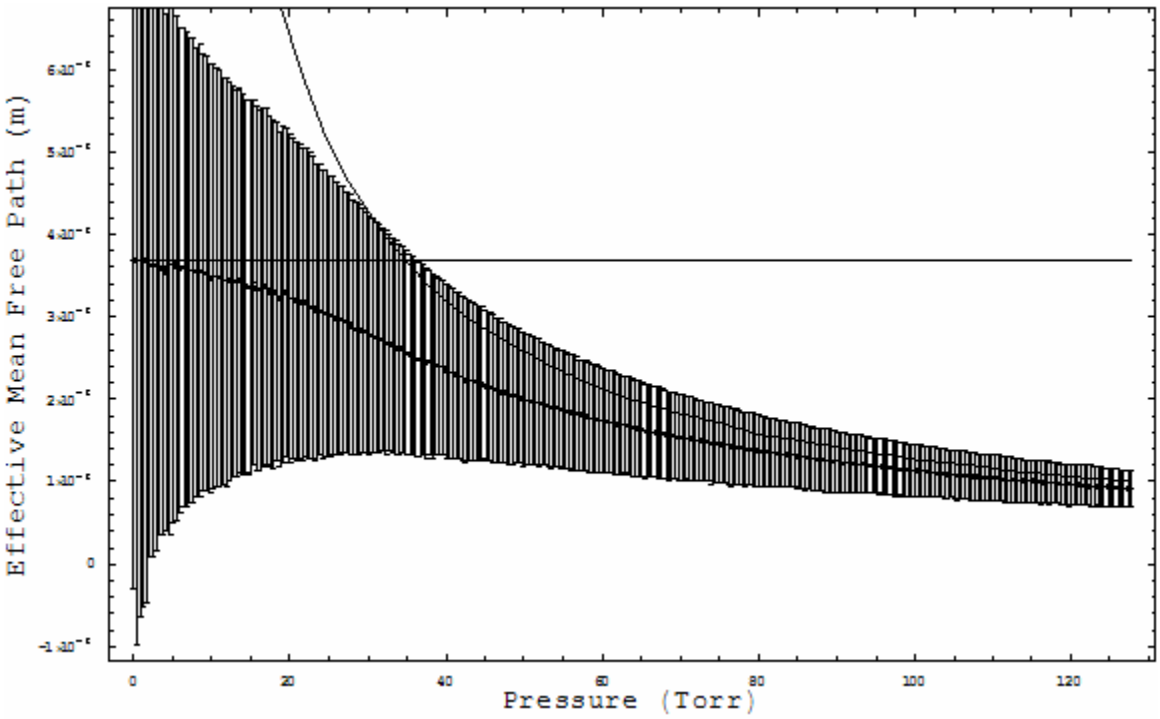

Figure 4.7. Pressure vs Effective Mean Free Path. The level of broadening is determined by both pressure and wall collisions.

We modeled the broadening mechanism inside the fiber to ensure our assumption that the dip was not overly broadened was reasonable. The results can be seen in Figure 4.7, but some explanation is warranted. To begin, the horizontal line indicates the mean free path of an unimpeded Cs atom bouncing between the walls of the fiber. The other function without error bars is the mean free path based on a Cs atom running into another atom, strictly determined by pressure. [8] The determination of the mean free path when both of these factors are included is fairly straightforward: as long as the fiber radius is much smaller than the mean free path of helium, as dictated by the pressure, then collision broadening will statistically dominate. On the other hand, if the pressure is high enough to cause the He mean free path to be shorter than the fiber radius then pressure broadening becomes more prevalent. In the region where they are both on the same order, a statistical approach is appropriate.

In order to accurately illustrate the transition from collision to pressure broadening dominance, we created an averaging loop based on some key assumptions. Given a random location in the fiber and a random velocity, the program would find how far a particular Cs atom traveled before it hit a wall and compared that number to the pressure dominated mean free path. The lesser of the two was annotated as the free path length for that random draw. This was repeated 50,000 times for each pressure. The mean and standard deviation are represented by the dark line and error bars in Figure 4.7. Initially, the fiber walls caused the collisions, but as the loop progressed through higher pressures the pressure dominated mean free path became the critical length. This mean free path was

$$\Lambda_{\text{var}} = \Lambda_{stp} \frac{P_{stp}}{P_{\text{var}}} \tag{4.12}$$

where Λ is the mean free path and P is pressure, where the subscripts represent either standard or variable conditions. Helium's mean free path changed as pressure increased, thus making pressure broadening more influential. [11] The fiber walls remained constant, initiating collision broadening only at low pressures. The error bars are a result of our statistical model, where the most significant room for error can be found near our starting point. The key point to garner from this model is that we were justified in assuming that our signal would not be broadened so drastically that we missed it in the recorded data, especially considering that our comparison leg was broadened by a pressure of one atmosphere and an effective mean free path much smaller than the fiber walls.

Another adjustment that might yield some success is to manufacture fiber with cesium in the core. Fibers are often made using a preform mold which maintains the cross-section profile of the desired fiber. This mold is stretched until the desired diameter is achieved. Putting cesium in the core of the mold is entirely possible, but the next hurdle would be using it in the lab. If the fiber tips were exposed to any water vapor whatsoever, both coupling and absorption would be reduced, if not eradicated entirely. Preparing the fiber would be virtually impossible using our current techniques, reducing the plausibility of this proposed solution.

The only other option is to completely redesign the experiment without fiber or capillary tubes. If we were to cover two plates in cesium, place micron spacers on the lower plate, and then lower the upper plate down until a seal was formed, we would have essentially formed a cavity similar to the one provided by the fiber. The

reason why this method is more attractive is because we know for certain that cesium is inside our cavity. Some foreseeable complications could be cesium leaking out of the cavity or our spacers and plates absorbing too much of the source laser light. The former could be remedied with optically clear spacers placed at either end of the cavity. The latter, on the other hand, could be made inconsequential if the cavity were small enough in relation to the laser power level; thus, we could still see a broadened dip even if a percentage of the power were absorbed by the plates.

After analyzing all of our options for getting cesium into the fiber, none of which proved to be very encouraging, we are confident that alterations must be made to the experimental design if the desired results are ever to be achieved.

V. Summary and Justification for Future Work

5.1 Summary

In this thesis I have demonstrated the ability to theoretically grasp a concept, design an experiment with a quantifiable goal, and build that experiment with an equivocal level of success. There are challenges to overcome in any project, but this project, containing so many variables both planned for and unforeseen, proved to be even more challenging than initially expected. Regardless of the cause for the various setbacks and alterations, the fact of the matter is that some worthwhile work was performed. The task of filling a hollow-core fiber with a gas is undoubtedly more difficult than originally conceived, but this realization would not have been made unless the theory had been applied. The fact that a clear absorption dip was viewed outside the fiber and then unnoticed when using the coupled light source is a significant piece of data that suggests many paths of continued experimentation.

5.2 Justification for Future Work

In my opinion, the most valuable result of my work is the plethora of possibilities for continued research on this topic. While my work did not conclusively prove or disprove the concept of collisionally broadening a laser source with a hollow-core fiber, it did clear away much of the fog surrounding the best way of designing and carrying out this task. The lack of hard, irrefutable data is not as disappointing when one considers the numerous suggestions that can be used to redesign this experiment and eventually attain the desired results. Specifically, a

mount redesign, using a capillary tube, manufacturing the fiber with cesium already contained in the core, or designing a cesium-coated plate system.

The quest for a high-energy laser is just as fervent now as when I began my thesis. My research, while not conclusive in itself, has paved the way for the next stage of this overall project. With some adjustments to the experiment, mainly concerning the ease of setup and the progress of cesium down the fiber, the question of using collision broadening to assist a high-energy laser can be explicitly answered.

Bibliography

1. "Photonic-Crystal Fiber".
   URL http://en.wikipedia.org/wiki/Photonic-crystal_fiber.

2. "HC-800-02: Hollow Core Photonic Bandgap Fiber." URL
   http://www.thorlabs.com/thorProduct.cfm?partNumber=HC-800-02

3. *Model 6300 User's Manual*. San Jose: New Focus, 2002.

4. *Model SR530 Lock-In Amplifier Manual*. Sunnyvale: Stanford Research Systems, 2001.

5. *Instruction Manual for Wavemeter*. Fishers: Burleigh, 1984.

6. *Pascal Series 2015 C2 Vacuum Pump Manual*. Annecy: Alcatel, 2001.

7. Al-Janabi, A. H. and E. Wintner. "Gaussian Laser Beam Propagation through Evacuated Hollow Core Photonic Crystal Fiber". IEEE, Mo B2.4 2005.

8. Bernath, Peter F. *Spectra of Atoms and Molecules, 2nd Edition*. Oxford University Press, 2005.

9. Bjarklev, A. et. Al., *Photonic Crystal Fibers.* Kluwer Academic Publishers, 2003.

10. Hect, Eugene. *Optics, 4th Edition*. Addison Wesley, 2002.

11. Jordan, Peter C. *Chemical Kinetics and Transport*. Plenum Press, 1979.

12. Perram, Glen P. *High Power Diode Pumped Alkali Vapor Lasers and Analog Systems*. AFIT/WPAFB. Paper and slides presented on 30 March 2007.

13. Rotondaro, Matthew D. and Glen P. Perram. "Collisional broadening and shift of the rubidium D_1 and D_2 lines $(5^2S_{1/2} \rightarrow 5^2P_{1/2}, 5^2P_{3/2})$ by rare gases, H_2, D_2, N_2, CH_4 and CF_4". *Journal of Quantitative Spectroscopy and Radiative Transfer*, Vol. 57, No. 4, 1997.

14. Rotondaro, Matthew D. and Glen P. Perram. "Role of rotational-energy defect in collisional transfer between the $5^2P_{1/2,3/2}$ levels in rubidium". *Physical Review*, May 1998.

15. Saleh, B.E.A. and M.C. Teich. *Fundamentals of Photonics, 2nd Edition*. John Wiley & Sons, 2007.

16. Tritton, D. J. *Physical Fluid Dynamics*. Van Nostrand Reinhold Co., 1977.

17. Verdeyen, J. T. *Laser Electronics, 3rd Edition*. Prentice Hall, 1994.

18. Zolla, F. et. Al. *Foundations of Photonic Crystal Fibers.* Imperial College Press, 2005.

REPORT DOCUMENTATION PAGE

Form Approved
OMB No. 074-0188

1. REPORT DATE *(DD-MM-YYYY)*	**2. REPORT TYPE**	**3. DATES COVERED** *(From – To)*
01-11-2007	Master's Thesis	Jun. 2007 – Sep. 2007

4. TITLE AND SUBTITLE

Collision Broadening Using Alkali-Filled, Hollow Core Fibers

5a. CONTRACT NUMBER

5b. GRANT NUMBER

5c. PROGRAM ELEMENT NUMBER

6. AUTHOR(S)

Rodgers, Luke P.

5d. PROJECT NUMBER

5e. TASK NUMBER

5f. WORK UNIT NUMBER

7. PERFORMING ORGANIZATION NAMES(S) AND ADDRESS(S)
Air Force Institute of Technology
Graduate School of Engineering and Management (AFIT/ENP)
2950 Hobson Way
WPAFB OH 45433-7765

8. PERFORMING ORGANIZATION REPORT NUMBER

AFIT/GAP/ENP/07-S01

9. SPONSORING/MONITORING AGENCY NAME(S) AND ADDRESS(ES)
Dr. Harro Ackermann
High Energy Laser – Joint Technology Office (HEL-JTO),
901 University Blvd. SE, Suite 100
Albuquerque, NM 87106

10. SPONSOR/MONITOR'S ACRONYM(S)

11. SPONSOR/MONITOR'S REPORT NUMBER(S)

12. DISTRIBUTION/AVAILABILITY STATEMENT
APPROVED FOR PUBLIC RELEASE; DISTRIBUTION UNLIMITED

13. SUPPLEMENTARY NOTES

14. ABSTRACT

The goal of this research was to demonstrate the possibility of collision broadening in a cesium-filled, hollow-core fiber as an alternative to the proven technique of pressure broadening. Theoretically, the absorption spectrum should collisionally broaden due to the presence of fiber walls. An absorption dip located at 852.34nm was recorded in a pressure broadened comparison leg. This data was used as a baseline during analysis of the fiber leg's data.

While the fiber was successfully exposed to the cesium under safe, controlled conditions, unexpected fluctuation in both the coupling efficiency and laser power levels resulted in the inability to record an absorption dip in the final data. As a result, an investigation of the fundamental assumptions and theory supporting this experiment was conducted. It was discovered that the current design does not provide an adequate opportunity for cesium to make its way into the fiber core, thus negating the possibility of achieving the desired collision broadening data. Recommendations are made as to how to improve this experiment for future study, founded on both theoretical calculations and experience gained in the lab.

15. SUBJECT TERMS
Collision Broadening, Laser, Fiber Optics, Spectroscopy

16. SECURITY CLASSIFICATION OF:			**17. LIMITATION OF ABSTRACT**	**18. NUMBER OF PAGES**	**19a. NAME OF RESPONSIBLE PERSON**
REPORT	**ABSTRACT**	**c. THIS PAGE**			**Maj Timothy H. Russell**
U	**U**	**U**	**UU**	77	**19b. TELEPHONE NUMBER** *(Include area code)* (937)-255-3636 EXT 7298 Timothy.Russell@AFIT.edu

Standard Form 298 (Rev: 8-98)
Prescribed by ANSI Std. Z39-18